complications of cyberknife have been reported (Table 1). Our patient developed a colonic apple-core lesion secondary to inflammatory changes after the cyberknife intervention. The presence of such a lesion proven to be nonmalignant has not been reported previously. It can be predicted that as more patients with unresectable abdominal malignancies, such as pancreatic carcinoma, are treated with cyberknife technology, more intra-abdominal radiation-induced complications will be recognized.

Although colonic apple-core lesions seen on radiology are considered to represent carcinoma unless proven otherwise, it is important to recognize that it may be caused by radiosurgery consequences. Although the future of cyberknife is promising, its complications should be considered when trying to minimize injury to the adjacent tissues.

ACKNOWLEDGMENTS

The authors thank Russel Saxton, MD, Mt Sinai, for his assistance with interpretations of the radiology films, and Tony Benito, photographer, Mt Sinai, for refining the quality of the images.

Roxane Scemla*
S. Mubashir Shah, MD†
Michael Schwartz, MD‡
Jamie S. Barkin, MD, MACG, FACP§
*Department of Gastroenterology
Ross University, School of Medicine/
Mt Sinai Medical Center
†Department of Gastroenterology
Mt Sinai Medical Center
‡Department of Oncology
Mt Sinai Medical Center
and §Division of Gastroenterology
University of Miami, School of Medicine/
Mt Sinai Medical Center Miami, Florida

REFERENCES

1. Chua YJ, Cunningham D. Adjuvant treatment for resectable pancreatic cancer. *J Clin Oncol*. 2005;23:4532–4537.
2. Randall B. Pancreatic cancer. *J Gastroenterol*. 2004;50:545–555.
3. Cheng Y, Gabor J, Zbigniew P. Measurements of the relative output factors for cyber knife collimators. *Neurosurgery*. 2004;54:157–162.
4. Cheng Y, Main W, Taylor D, et al. An anthropomorphic phantom study of the accuracy of cyberknife spinal radiosurgery. *Neurosurgery*. 2004;55:1138–1145.
5. Friedman W. Linear accelerator–based radiosurgery for vestibular schwannoma. *Neurosurg Focus*. 2003;14:2.
6. Pollock B. Stereotactic radiosurgery for intracranial meningiomas: indications and results. *Neurosurg Focus*. 2003;14:2.
7. Chua D, Shan J, Kwong P, et al. Linear accelerator–based stereotactic radiosurgery for locally persistent and recurrent nasopharyngeal carcinoma: efficacy and complications. *Int J Radiat Oncol Biol Phys*. 2003;56:177–183.
8. Lee S, Choi E, Park H, et al. Stereotactic body frame based on radiosurgery on consecutive for primary or metastatic tumors on lung. *Strahlenther Onkol*. 2003;40:309–315.
9. Benzyl D, Saboori M, Mogilner A, et al. Safety and efficacy of stereotactic radiosurgery for tumors of the spine. *J Neurosurg*. 2004;101:413–418.
10. Pham C, Chang S, Jones P, et al. Preliminary visual field preservation after stage cyberknife radiosurgery for perioptic lesions. *Neurosurgery*. 2004;54:799–812.

Imaging Features of Large Intraductal Papillary Mucinous Carcinoma of the Pancreatic Tail

Abbreviations: IPMT, intraductal papillary mucinous tumor, MCT, mucinous cystic tumor, US, ultrasound, CT, computed tomography, MPD, main pancreatic duct, MRCP, magnetic resonance cholangiopancreatography

To the Editor:

Pancreatic mucin-producing tumors, such as intraductal papillary mucinous tumor (IPMT) and mucinous cystic tumor (MCT),[1,2] are good candidates for surgical resection because of their low-grade malignant potential. It is sometimes difficult to differentiate between IPMT and MCT on imaging studies because the 2 entities sometimes show similar cystic findings. We encountered 2 patients with a large malignant IPMT in the pancreatic tail, which showed common impressive imaging features and similar pathological findings.

CASE 1

A 68-year-old man with no symptom was admitted to our department with the diagnosis of a pancreatic tumor. Ultrasound (US) showed a large, pear-shaped, low-echoic lesion between the stomach and spleen. In the cystic lesion, numerous echogenic lines with spontaneous wavelike movements were seen (Fig. 1A). Dynamic computed tomography (CT) scan demonstrated a large, pear-shaped cystic tumor, 13 cm in diameter, with multilocular margins on its caudal part in the tail of the pancreas. The edge of the pancreatic parenchyma was deformed into a beak shape ("beak sign"),[3] which represented a firm continuity of the tumor with the main pancreatic duct (MPD) (Fig. 1B). Magnetic resonance cholangiopancreatography (MRCP) demonstrated a very high-intensity mass with numerous streaks along the major axis, referred hereafter as a "brushing sign," which was thought to represent the mucinous component of the tumor. Several cystic dilatations of the branch duct in the head and body of the pancreas were also found (Fig. 1C). The preoperative diagnosis was multicentric IPMTs, one of which exhibited a tremendous growth in the tail of the pancreas. Distal pancreatectomy was performed. The histological finding was intraductal papillary mucinous carcinoma with invasion slightly beyond the duct wall, that is, with minimal invasion [4,5] (Fig. 1D). In the mucus pool of the markedly dilated MPD, the tumor cells were peeled off and floating with their corpses.

CASE 2

A 61-year-old woman who had repeated pancreatitis was referred to our department for the treatment of a large cystic tumor in the tail of the pancreas. On US, a large low-echoic lesion was visualized in a spindle form, and numerous echogenic streaming patterns were seen therein. A CT scan revealed a large low-attenuating tumor, 13 × 5 cm in size, in the tail of the pancreas. A beak sign was also found in the tail of the pancreas. Several mural nodules suggested the presence of malignant component. On MRCP, the brushing signs were also observed within the cystic tumor. Distal pancreatectomy was performed. The pathological diagnosis was intraductal papillary mucinous carcinoma with minimal invasion.

A differential diagnosis between IPMT and MCT is sometimes difficult. Both tumors can contain mucinous components and have malignant potentials, especially when the tumor has mural nodules or solid components.[6] IPMT is located in the pancreatic head in 60% of patients and sometimes exhibits intraductal spread[7] or multicentric occurrence along MPD[8] and is continuous with the MPD.[6] On the other hand, MCT arises from the pancreatic tail in

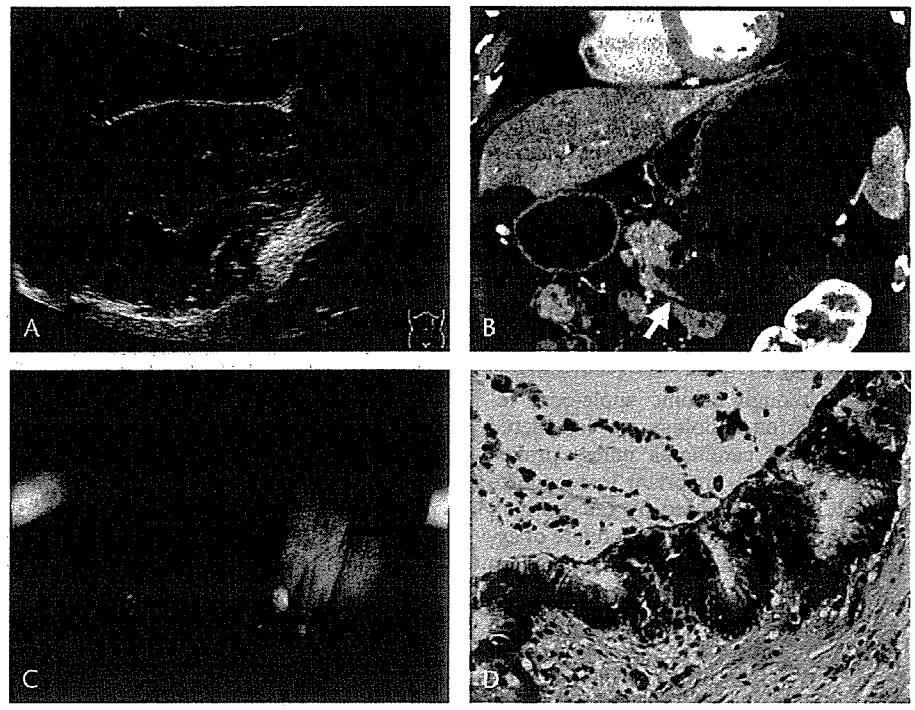

FIGURE 1. A, Abdominal US shows numerous streaming lines that spontaneously move in a wavelike manner inside the cystic tumor in a sagittal direction. B, Coronal reformatted CT scan reveals "a beak sign" (arrow) between the cystic tumor of the pancreatic tail and the MPD. C, MRCP shows a very high-intensity mass with "a brushing sign" inside the tumor of the pancreatic tail. Several cystic lesions are also present in the head and body of the pancreas. D, The irregular papillary projections are composed of tall columnar cells with nuclear atypia, and part of the tumor has collapsed, forming the streaked structures in the mucous pool with epithelial corpses (upper left, hematoxylin-eosin, magnification ×200).

70% to 90% of patients,[6,9] with a higher prevalence in women,[1,2] and is rarely continuous with MPD.[5] MCT can be pathologically characterized as ovarian-type stroma.[2] In the present cases, multicentric occurrence in CASE 1 and mural nodule in CASE 2 also suggested IPMT rather than MCT.

The impressive common imaging features of the 2 megacystic lesions were (1) a beak sign on CT images, suggesting a pancreatic origin and the distinct continuity of the cystic part with MPD, and (2) a brushing sign on MRCP, which might express moving mucinous components with a large amount of peeled epithelium and their corpses, floating inside the tumor. In the diagnosis of megacystic tumor in the tail of the pancreas, the beak sign and brushing sign might be helpful to differentiate IPMT from MCT.

Yu Takahashi, MD*
Yoshihiro Sakamoto, MD*
Kazuaki Shimada, MD*
Tsuyoshi Sano, MD*
Tomoo Kosuge, MD*
Hiroaki Onaya, MD†
Yasunori Mizuguchi, MD†
Nobuyoshi Hiraoka, MD‡
*Hepatobiliary and Pancreatic Surgery Division
†Diagnostic Radiology Division; and
‡Pathology Division
National Cancer Center Research Institute
Tokyo, Japan

REFERENCES

1. Klöppel G, Solcia E, Longnecker DS, et al. Histological typing of tumors of the exocrine pancreas. In: *WHO International Histological Classification of Tumors*, 2nd ed. New York: Springer-Verlag; 1996.
2. Solica E, Capella C, Klöppel G. Tumors of the pancreas. *Atlas of Tumor Pathology, 3rd series, Fascicle 20*. Washington, DC: Armed Forces Institute of Pathology; 1997.
3. Nishino M, Hayakawa K, Minami M, et al. Primary retroperitoneal neoplasms: CT and MR imaging findings with anatomic and pathologic diagnostic clues. *Radiographics*. 2003;23:45–57.
4. Fukushima N, Mukai K, Kanai Y, et al. Intraductal papillary tumors and mucinous cystic tumors of the pancreas: clinicopathologic study of 38 cases. *Hum Pathol*. 1997;28: 1010–1017.
5. Zamboni G, Scarpa A, Bogina G, et al. Mucinous cystic tumors of the pancreas. Clinicopathological features, prognosis, and relationship to other mucinous cystic tumors. *Am J Surg Pathol*. 1999;23:410–422.
6. Sugiyama M, Atomi Y. Intraductal papillary mucinous tumors of the pancreas. Imaging studies and treatment strategies. *Ann Surg*. 1998;228:685–691.
7. Fukushima N, Mukai K. Differential diagnosis between intraductal papillary-mucinous tumors and mucinous cystic tumors of the pancreas. *Int J Surg Pathol*. 2000;8: 271–278.
8. Obara T, Saitoh Y, Maguchi H, et al. Multicentric development of pancreatic intraductal carcinoma through atypical papillary hyperplasia. *Hum Pathol*. 1992;23:82–85.
9. Sarr MG, Carpenter HA, Prabhakar LP, et al. Clinical and pathologic correlation of 84 mucinous cystic neoplasms of the pancreas. Can one reliably differentiate benign from malignant (or premalignant) neoplasms? *Ann Surg*. 2000;231:205–212.

British Journal of Cancer (2006) 95, 601 – 606

www.bjcancer.com

NK105, a paclitaxel-incorporating micellar nanoparticle, is a more potent radiosensitising agent compared to free paclitaxel

T Negishi[1], F Koizumi[1], H Uchino[2], J Kuroda[1], T Kawaguchi[3], S Naito[2] and Y Matsumura*[,1]

[1]Investigative Treatment Division, Research Center for Innovative Oncology, National Cancer Center Hospital East, 6-5-1 Kashiwanoha, Kashiwa, Chiba 277-8577, Japan; [2]Department of Urology, Graduate School of Medical Sciences, Kyushu University, 3-1-1 Maidashi, Higashi-ku, Fukuoka, Fukuoka 812-8582, Japan; [3]Department of Anatomy and Histology, Fukushima Medical University School of Medicine, 1-Hikariga-oka, Fukushima, Fukushima 960-1247, Japan

NK105 is a micellar nanoparticle formulation designed to enhance the delivery of paclitaxel (PTX) to solid tumours. It has been reported to exert antitumour activity *in vivo* and to have reduced neurotoxicity as compared to that of free PTX. The purpose of this study was to investigate the radiosensitising effect of NK105 in comparison with that of PTX. Lewis lung carcinoma (LLC)-bearing mice were administered a single intravenous (i.v.) injection of PTX or NK105; 24 h after the drug administration, a proportion of the mice received radiation to the tumour site or lung fields. Then, the antitumour activity and lung toxicity were evaluated. In one subset of mice, the tumours were excised and specimens were prepared for analysis of the cell cycle distribution by flow cytometry. Combined NK105 treatment with radiation yielded significant superior antitumour activity as compared to combined PTX treatment with radiation ($P = 0.0277$). On the other hand, a histopathological study of lung sections revealed no significant difference in histopathological changes between mice treated with PTX and radiation and those treated with NK105 and radiation. Flow-cytometric analysis showed that NK105-treated LLC tumour cells showed more severe arrest at the G2/M phase as compared to PTX-treated tumour cells. The superior radiosensitising activity of NK105 was thus considered to be attributable to the more severe cell cycle arrest at the G2/M phase induced by NK105 as compared to that induced by free PTX. The present study results suggest that further clinical trials are warranted to determine the efficacy and feasibility of combined NK105 therapy with radiation.
British Journal of Cancer (2006) **95,** 601 – 606. doi:10.1038/sj.bjc.6603311 www.bjcancer.com
Published online 8 August 2006

Keywords: paclitaxel; NK105; radiosensitiser; polymer micelle; drug delivery system

Paclitaxel (PTX) has been demonstrated to be one of the most effective anticancer agents available at present (Carney, 1996; Khayat *et al*, 2000). Besides its antitumour activity, its ability to induce radiosensitisation has been reported both *in vitro* (Tishler *et al*, 1992; Choy *et al*, 1993; Lokeshwar *et al*, 1995; Rodriguez *et al*, 1995) and *in vivo* (Milas *et al*, 1994, 1995; Cividalli *et al*, 1998) this effect has been attributed to its effect of stabilising microtubules and inducing cell cycle arrest at the G2/M phase, the most radiosensitive phase of the cell cycle (Terasima and Tolmach, 1963; Sinclair and Morton, 1966). As several clinical studies have demonstrated the efficacy of PTX-based chemotherapy combined with radiotherapy, the combined modality is considered to be a potentially important treatment option for lung and breast cancer (Choy *et al*, 1998a, b, 2000; Dowell *et al*, 1999; Formenti *et al*, 2003; Kao *et al*, 2005).

The adverse effects of radiation, namely, lung toxicities in patients with breast or lung cancer treated by thoracic radiation, are of great concern, and may be dose limiting or even have a negative impact on the quality of life of the patients, even though radiation is an efficient treatment option. Lung toxicities often result in lung fibrosis, necessitating change of the treatment method and causing much distress or even death of the patients (Penney and Rubin, 1977; Early Breast Cancer Trialists' Collaborative Group, 2000; Lind *et al*, 2002). Some clinical trials actually reported an increased incidence of pneumonitis following combined PTX therapy with radiation in patients with breast or lung cancer (Taghian *et al*, 2001; Hanna *et al*, 2002; Chen and Okunieff, 2004).

Although widely used, PTX itself has several adverse effects, such as peripheral sensory neuropathy (Rowinsky *et al*, 1993; Rowinsky and Donehower, 1995), and its poor solubility in water is also associated with such effects as anaphylaxis and other severe hypersensitivity reactions attributable to Cremophor EL and ethanol, which are essential for solubilising PTX (Weiss *et al*, 1990; Rowinsky and Donehower, 1995). In order to overcome these problems, we prepared a new formulation, NK105, which is a PTX-incorporating polymeric micellar nanoparticle (85 nm in size) (Hamaguchi *et al*, 2005). NK105 is formed by facilitating the self-association of amphiphilic block copolymers constructed using polyethylene glycol (PEG) as the hydrophilic segment and modified polyaspartate as the hydrophobic segment in an aqueous medium. Owing to the PEG constituting the outer shell of the micelles, NK105 is soluble in water. In addition, PEG also confers a stealth property to the formulation, that allows the micellar drug preparation to be less avidly taken up by the reticuloendothelial

*Correspondence: Dr Y Matsumura; E-mail: yhmatsum@east.ncc.go.jp
Revised 5 June 2006; accepted 11 July 2006; published online 8 August 2006

system (RES) and to be retained in the circulation for a longer period of time (Klibanov *et al*, 1990, 1991; Allen, 1994; Gabizon *et al*, 1996). The prolonged circulation time and the ability of NK105 to extravasate through the leaky tumour vasculature (i.e., the EPR (enhanced permeability and retention) effect) causes accumulation of PTX in tumour tissues (Matsumura and Maeda, 1986; Maeda and Matsumura, 1989). We previously demonstrated that NK105 is associated with reduced neurotoxicity and also exerts more potent antitumour activity on human cancer xenograft, as compared to free PTX. In addition, because of its solubility in water, it is expected that the incidence of anaphylaxis and hypersensitivity reactions attributable to Cremophor EL and ethanol may also be reduced with NK105. A clinical trial of NK105 is now under way.

In this context, it is expected that the use of NK105 in place of PTX in combination with radiation may also yield superior results, because of the more potent antitumour activity of this drug as compared to that of free PTX. In this study, we evaluated the antitumour activity and severity of lung fibrosis induced by PTX and NK105 administered in combination with thoracic radiation, to examine whether combined NK105 chemotherapy with radiation would be an acceptable or useful treatment modality.

MATERIALS AND METHODS

Mice

Eight-week-old female C57BL/6J mice were purchased from Charles River Japan Inc. (Kanagawa, Japan). All the animal procedures were performed in compliance with the guidelines for the care and use of experimental animals, drawn up by the Committee for Animal Experimentation of the National Cancer Center; these guidelines meet the ethical standards required by law and also comply with the guidelines for the use of experimental animals in Japan.

PTX and NK105

Paclitaxel was purchased from Merican Corp. (Tokyo, Japan). NK105 is a PTX-incorporating 'core-shell-type' polymeric micellar nanoparticle formulation that was prepared by a previously reported procedure (Hamaguchi *et al*, 2005). Briefly, polymeric micellar particles were formed by facilitating the self-association of amphiphilic block copolymers in an aqueous medium. The polymer of NK105 was constructed using PEG as the hydrophilic segment and modified polyaspartate as the hydrophobic segment. The carboxylic groups of the polyaspartate block were modified by the esterification reaction with 4-phenyl-1-butanol, resulting in conversion of half of the groups to 4-phenyl-1-butanolate. Molecular weight of the polymers was determined to be approximately 2000 (PEG block: 12 000; moditied polyaspartate block: 8000).

Via the self-association process, PTX was incorporated into the inner core of the micelle system by physical entrapment through hydrophobic interactions between the drug and specifically well-designed block copolymers for PTX. NK105 was obtained as a freeze-dried formulation and contained ca.23% (WW^{-1}) of PTX. Finally, NK105, PTX-incorporating polymeric micellar nanoparticle formulation with a single and narrow size distribution, was obtained. The weight-average diameter of the nanoparticles was approximately 85 nm ranging from 20 to 430 nm.

Irradiation

The mice were anesthetised by intraperitoneal (i.p.) injection of nembutal (75 mg kg^{-1}) and placed on the stage for irradiation. The whole thorax or subcutaneous (s.c.) tumours of the thigh were irradiated using a Faxitron cabinet X-ray system model CP-160 by 100 kV X-rays from a linear accelerator, at a dose rate of 2 Gy min^{-1}. Totally 12 Gy was irradiated to each mouse. The whole body except irradiated parts, lung field or tumour lesion, were shielded with specially designed lead blocks.

Flow cytometry

At 24 h after the injection of PTX or NK105 into the Lewis lung carcinoma (LLC) tumour-bearing C57BL/6j mice, the tumours were excised, minced in PBS, and fixed in 70% ethanol at 4°C for 48 h. After being fixed, the tumours were digested with 0.04% pepsin (Sigma chemical co., St Louis, MO, USA) in 0.1 N HCl for 60 min at 37°C in a shaking bath for preparing single-nuclei suspensions. The nuclei were then centrifuged, washed twice with PBS, and stained with 40 $\mu g\,ml^{-1}$ of propidium iodide (Molecular Probes, OR, USA) in the presence of 100 $\mu g\,ml^{-1}$ RNase in 1 ml PBS for 30 min at 37°C. The stained nuclei were analysed with a B-D FACSCalibur (BD Biosciences, San Jose, CA, USA). The cell cycle distribution was analysed using the Modfit program (Verity Software House Inc., Topsham, ME, USA).

Evaluation of the antitumour activity

For this experiment, 3×10^6 LLC cells were inoculated s.c. into the right thighs of mice. The tumour volume was calculated using the formula, tumour volume (mm^3) $= a \times b^2/2$ (a = longest tumour diameter, b = shortest tumour diameter). When the tumour volume reached approximately 100 mm^3 on day 14 after the tumour inoculation, the mice were randomly allocated to test groups of about four or five mice each, and started the treatment on the same day. There were six test groups, as follows: untreated control, PTX treatment alone, NK105 treatment alone, radiation alone, combined PTX treatment with radiation, and combined with NK105 treatment with radiation.

In the groups receiving PTX or NK105, the mice were administered a single intravenous (i.v). injection of PTX or NK105 at the dose of 45 mg kg^{-1}; 24 h after the drugs were administered, the tumour sites of the mice in the groups scheduled to receive radiation were irradiated.

The antitumour activity of each treatment regimen was evaluated by measuring the tumour volume. Tumour volume and body weight was measured every 3 days.

Evaluation of lung toxicity

The severity of lung toxicity was evaluated histologically in the following test groups; untreated control ($n = 6$), radiation treatment alone ($n = 6$), combined PTX treatment with radiation ($n = 9$), and combined NK105 treatment with radiation ($n = 10$). Mice were administered a single i.v. injection of PTX or NK105 at the dose of 45 mg kg^{-1}; 24 h after the drugs were administered, the thorax of the mice in the groups scheduled to receive radiation was irradiated. All the mice were killed 36 weeks after the drug administration. At the time of the killing, the lungs were removed, and the right lungs were fixed in 10% buffered formalin for 24 h, then embedded in paraffin. The lungs were inflated at 20 cm water pressure by intratracheal infusion of 10% buffered formalin before fixation. Sections (5 μm- thick) were stained with haematoxylin and eosin (H&E) and observed under the light microscope. The severity of the pulmonary fibrosis was assessed based on Ashcroft's scoring system (Ashcroft *et al*, 1988). Briefly, all the fields of each lung section were scanned under a Leica microscope at a magnification of $\times 100$, then each field was visually graded from 0 (normal lung) to 8 (total fibrotic obliteration of the field). The mean grades obtained for all of the fields was then calculated as the visual fibrotic score.

Immunohistochemistry

The lung sections were deparaffinised and rehydrated, then microwaved in 0.01 M sodium citrate buffer for 15 min at 90°C to retrieve epitopes, and cooled at room temperature. An endogenous peroxidase blocking solution of 3% hydrogen peroxide was applied for 20 min at room temperature. After blocking the nonspecific binding sites with 2% normal goat serum, the sections were incubated with rabbit anti-mouse collagen III immunoglobulin G (IgG) (Chemicon International, Temecula, CA, USA) overnight at 4°C. The sections were then washed with PBS, followed by the addition of biotin-conjugated goat anti-rabbit IgG (Vector Laboratories Inc., Burlingame, CA, USA) and incubation for 30 min at room temperature. The sections were then washed and incubated with horseradish-peroxidase-conjugated avidin–biotin complex (Vector Laboratories Inc., Burlingame, CA, USA) at room temperature for 30 min, in accordance with the manufacturer's instructions (Vector Laboratories Inc.). The immunoreactions were visualised using 3,3′-diaminobenzidine as the substrate and counterstaining with haematoxylin.

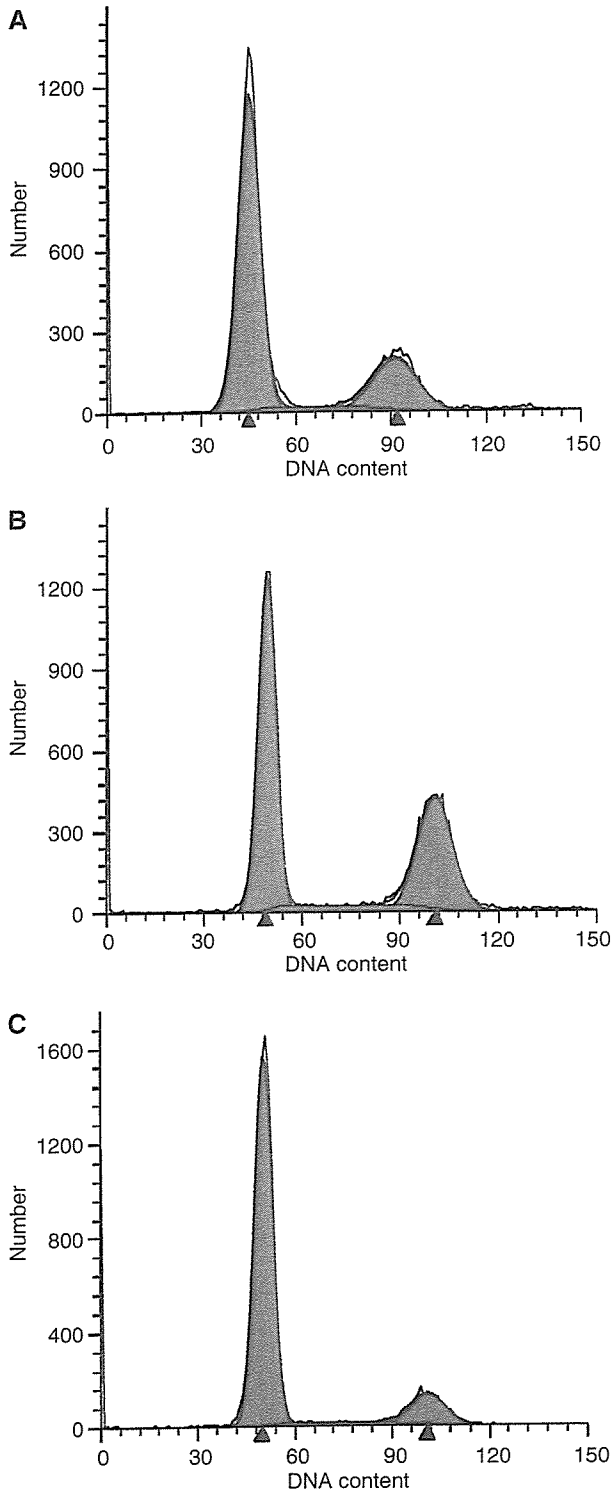

Figure 1 Cell cycle analysis. Cell cycle analysis of LLC tumour cells 24 h after PTX (**A**) or NK105 administration (**B**). Untreated control cells are shown in (**C**).

Statistical analysis

Date were expressed the mean ± s.d. Differences between the test groups were analysed by Student's *t*-test. We used Stat View (SAS Institute Inc.) statistical software. A value of $P<0.05$ was considered statistically significant.

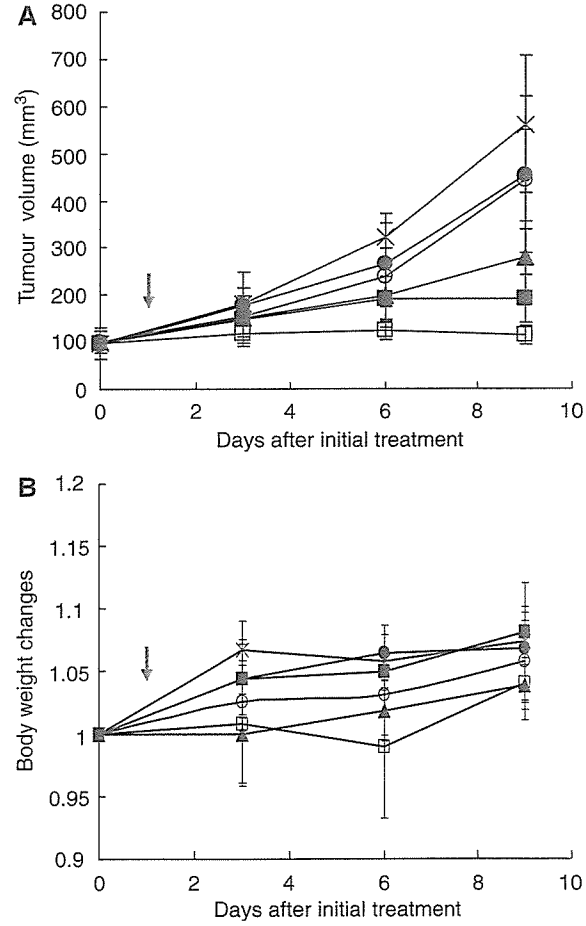

Figure 2 Antitumour activity. Changes in the LLC tumour growth rates in the mice. (**A**) Mice receiving TXL-alone (●), NK105-alone (○), combined treatment with PTX and radiation (■), and combined treatment with NK105 and radiation (□) were administered a single i.v. injection of PTX or NK105 at the dose 45 mg kg^{-1} on day 14 after the tumour inoculation (= on day 0 after the initial treatment). After 24 h the drugs were administered, the mice in the radiation-alone (△) and the combined-treatment groups were irradiated (arrow). Mice in the control group (×) were given no treatment. (**B**) Changes in the relative body weight. Data were derived from the same mice as those used in the present study.

RESULTS

Cell cycle analysis

At 24 h after the administration of PTX or NK105 to the LLC-tumour-bearing mice, severe cell cycle arrest at the G2/M phase was observed in the tumour cells treated with the drugs as compared with that in the control (no drug treatment) (Figure 1C). There was a tendency towards the NK105-treated LLC tumour cells (Figure 1B) showing more severe arrest at the G2/M phase than the PTX-treated cells (Figure 1A).

Antitumour activity

Decreased tumour growth rates of the LLC tumours were observed in the mice of the radiation alone, combined PTX with radiation, and combined NK105 with radiation groups. No antitumour activity was observed following treatment with either PTX or NK105 alone, because LLC is primarily a PTX-resistant tumour. Combined NK105 therapy with radiation yielded superior antitumour activity as compared to both radiation alone ($P = 0.0047$) and combined PTX therapy with radiation ($P = 0.0277$) on the day 9 after the treatment initiation (Figure 2A). No significant differences in body weight changes were noted among the groups tested (Figure 2B).

Lung toxicities

Histopathological examination of the lung sections of all the mice receiving radiation showed inflammatory cell infiltration, appearance of intra-alveolar macrophages, and destruction of the alveolar architecture. Major portions of the alveolar septa in the lung sections prepared from the irradiated mice showed slight thickening, although no massive structural destruction was observed (Figure 3A). On the other hand, the lung sections prepared from the control nonirradiated group showed no significant histopathological changes (Figure 3B). Ashcroft's fibrosis scores in the groups of mice that received radiation ranged from 0.975 to 1.426, with no significant differences among the groups. The score in the control group was nearly zero. In the groups receiving radiation, the severity of lung fibrosis differed significantly among the mice within the same groups, as did the Ashcroft's scores, that is, the s.d. of the Ashcroft's scores in the mice receiving radiation was very high (Figure 3C).

Type III collagen deposition

Immunohistochemical analysis of lung sections prepared from the mice receiving radiation revealed significant collagen deposition, especially in the subpleural regions, while that of lung sections prepared from the control group showed little collagen deposition. There were no significant differences among the different groups receiving radiation (Figure 3D).

DISCUSSION

It is well known that PTX enhances the radiosensitivity of tumour cells by inducing cell cycle arrest at the G2/M phase, the most radiosensitive phase of the cell cycle (Terasima and Tolmach, 1963;

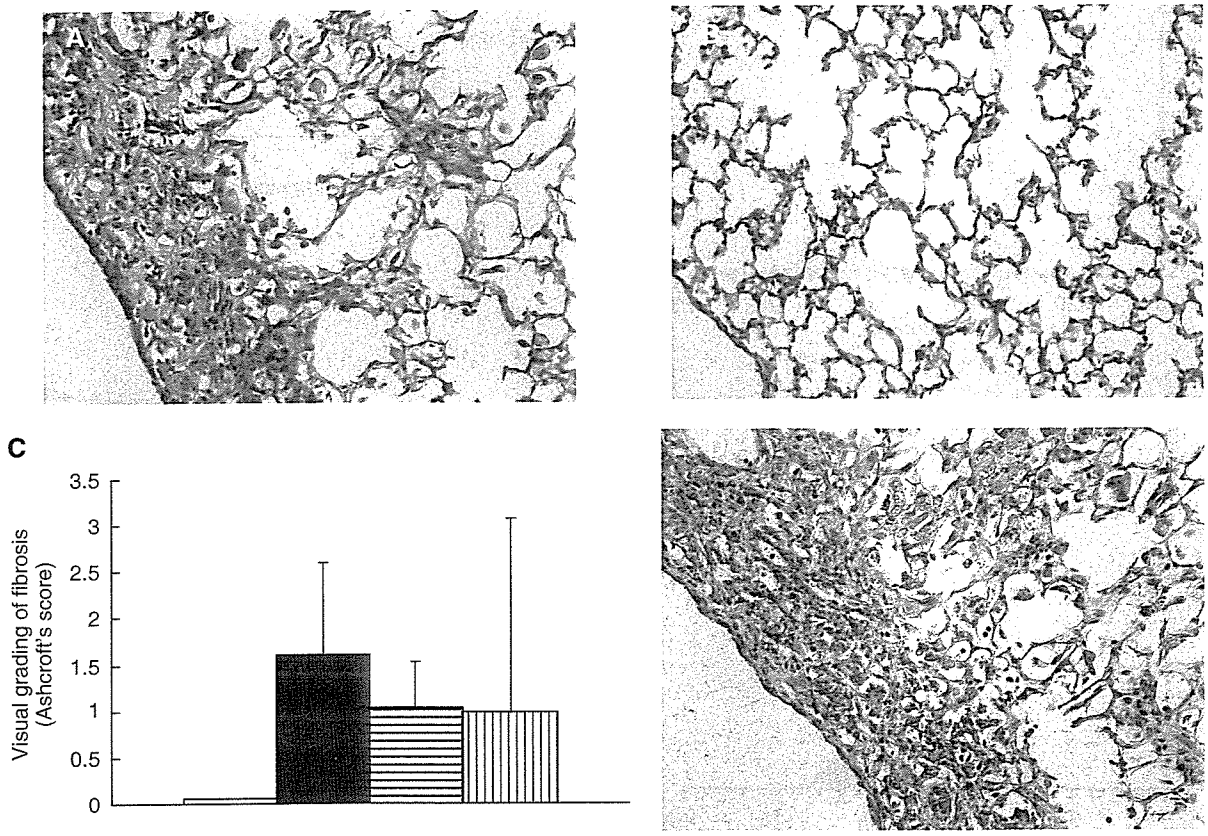

Figure 3 H&E staining of the lungs of C57BL/6J mice surviving 36 weeks after the thoracic radiation (**A**) and sham radiation (**B**). (**C**) Semiquantitative analyses to estimate the severity of pulmonary fibrosis in the mice receiving sham radiation (□), thoracic radiation alone (■), combined PTX with radiation (▤), and combined NK105 with radiation (▥). H&E- stained lung tissue sections were assessed to estimate the severity of pulmonary fibrosis by visual grading of fibrosis (Ashcroft's score). Collagen III staining of the irradiated lungs of mice (**D**).

Sinclair and Morton, 1966). Many reports have confirmed the radiosensitising effect of PTX in different cell lines (Tishler *et al*, 1992; Choy *et al*, 1993; Lokeshwar *et al*, 1995; Rodriguez *et al*, 1995), *in vivo* experiments (Milas *et al*, 1994, 1995; Cividalli *et al*, 1998), and in several clinical trials of combined PTX with radiation therapy according to different schedules (Dillman *et al*, 1990; Arriagada *et al*, 1991; Morton *et al*, 1991; Furuse *et al*, 1999; Sause *et al*, 2000; Chen *et al*, 2003). Chen *et al* (2003) examined the optimal timing of PTX treatment and irradiation in relation to the cell cycle, and recommended that radiation be given at least 5 h after PTX administration, because G2/M arrest of a lung cancer cell line was shown to start at 4 h after PTX treatment and to last for 44 h.

In our experimental model to evaluate the antitumour activity, the tumours were irradiated 24 h after a single i.v. injection of PTX or NK105. No significant increase in the antitumour activity as compared with that in the control (no treatment) was observed following a single i.v. injection of either PTX or NK105 at the dose of 45 mg kg^{-1}; LLC tumours are known to be primarily resistant to PTX. In fact, the IC_{50} of PTX against an LLC tumour cell line was shown to be 84.1 nM, which is about 10-fold higher than that of NK105 against various cancer cell lines tested in our previous work (Hamaguchi *et al*, 2005). Combined NK105 therapy with radiation yielded superior antitumour activity as compared with radiation alone or combined PTX therapy with radiation. This result suggests that NK105 has a more potent radiosensitising effect than PTX. In our study, there was a tendency towards NK105-treated LLC tumour cells showing more severe arrest at the G2/M phase as compared to PTX-treated cells at 24 h after the injection of the drugs, the timing of the radiation treatment, probably because NK105 allows a higher concentration of PTX to be maintained in the tumour than conventional PTX (Hamaguchi *et al*, 2005). We suppose that this is the reason why NK105 exerted more potent radiosensitising activity than PTX.

Next, we were concerned about the adverse effects of combined NK105 therapy with radiation. New micellar drugs are designed based on the idea that DDS can accumulate in the tumour selectively, while showing reduced distribution in normal tissues. We demonstrated that the incorporation of cisplatin into micelles significantly reduced the nephrotoxicity and neurotoxicity of cisplatin (Uchino *et al*, 2005). However, it was also shown that micelle- incorporated cisplatin caused transient liver dysfunction because it was trapped more avidly by the RES as compared to free cisplatin, even though the PEG of the outer shell of the micelle confers the so-called stealth effect.

In this study, our examination of the lung sections of mice treated with NK105 and radiation revealed that the histopathological changes such as inflammatory cell infiltration, appearance of intra-alveolar macrophages, and destruction of the alveolar architecture were induced by thoracic radiation and not by the accumulation of NK105 in the lung. There were no significant differences in the histopathological changes observed among the mice treated by NK105 and radiation and mice treated by radiation alone or PTX with radiation. The severity of lung fibrosis did not differ significantly among the test groups either. Although some clinical trials reported an increased incidence of pneumonitis and esophagitis following combined PTX therapy with radiation (Taghian *et al*, 2001; Hanna *et al*, 2002; Chen and Okunieff, 2004), others reported no influence on the incidence of such adverse effects (Ellerbroek *et al*, 2003; Yu *et al*, 2003). Several clinical trials and *in vivo* experiments have discussed the subject, however, no definitive conclusion has been arrived at (Mason *et al*, 1995; Choy *et al*, 1998; Yu *et al*, 2004; Kao *et al*, 2005). In our study, in regard to the incidence of esophagitis, there were no significant differences in the histopathological changes observed in the esophageal sections at one week after the treatment among the test groups (data not shown).

In conclusion, we demonstrated that combined NK105 chemotherapy with radiation exerts significant antitumour activity. Furthermore, the lung toxicity of this combined treatment modality was also acceptable as compared with that observed following radiation alone or combined PTX therapy with radiation. However, further studies are necessary to determine the effectiveness of NK105 in terms of its radiosensitising effect.

ACKNOWLEDGEMENTS

We thank Drs K Sugiyama and K Tsuchihara for their scientific advice and Mrs C Kanai and Mrs N Mie for their technical assistance. We are also grateful to Mrs K Shiina for her secretarial assistance. This work was supported by a Grant-in-Aid from the Ministry of Health, Labor and Welfare of Japan (Y Matsumura) and a Grant-in-Aid for Scientific Research on Priority Areas from the Ministry of Education, Culture, Sports, Science and Technology (Y Matsumura).

REFERENCES

Allen TM (1994) Long-circulating (sterically stabilized) liposomes for targeted drug delivery. *Trends Pharmacol Sci* **15:** 215–220

Arriagada R, Le Chevalier T, Quoix E, Ruffie P, de Cremoux H, Douillard JY, Tarayre M, Pignon JP, Laplanche A (1991) ASTRO (American Society for Therapeutic Radiology and Oncology) plenary: Effect of chemotherapy on locally advanced non-small cell lung carcinoma: a randomized study of 353 patients. GETCB (Groupe d'Etude et Traitement des Cancers Bronchiques), FNCLCC (Federation Nationale des Centres de Lutte contre le Cancer) and the CEBI trialists. *Int J Radiat Oncol Biol Phys* **20:** 1183–1190

Ashcroft T, Simpson JM, Timbrell V (1988) Simple method of estimating severity of pulmonary fibrosis on a numerical scale. *J Clin Pathol* **41:** 467–470

Carney DN (1996) Chemotherapy in the management of patients with inoperable non-small cell lung cancer. *Semin Oncol* **23:** 71–75

Chen Y, Okunieff P (2004) Radiation and third-generation chemotherapy. *Hematol Oncol Clin North Am* **18:** 55–80

Chen Y, Pandya K, Keng PC, Johnstone D, Li J, Lee YJ, Smudzin T, Okunieff P (2003) Phase I/II clinical study of pulsed paclitaxel radiosensitization for thoracic malignancy: a therapeutic approach on the basis of preclinical research of human cancer cell lines. *Clin Cancer Res* **9:** 969–975

Choy H, Akerley W, Safran H, Graziano S, Chung C, Williams T, Cole B, Kennedy T (1998a) Multiinstitutional phase II trial of paclitaxel, carboplatin, and concurrent radiation therapy for locally advanced non-small-cell lung cancer. *J Clin Oncol* **16:** 3316–3322

Choy H, Devore III RF, Hande KR, Porter LL, Rosenblatt P, Yunus F, Schlabach L, Smith C, Shyr Y, Johnson DH (2000) A phase II study of paclitaxel, carboplatin, and hyperfractionated radiation therapy for locally advanced inoperable non-small-cell lung cancer (a Vanderbilt Cancer Center Affiliate Network Study). *Int J Radiat Oncol Biol Phys* **47:** 931–937

Choy H, Rodriguez FF, Koester S, Hilsenbeck S, Von Hoff DD (1993) Investigation of taxol as a potential radiation sensitizer. *Cancer* **71:** 3774–3778

Choy H, Safran H, Akerley W, Graziano SL, Bogart JA, Cole BF (1998b) Phase II trial of weekly paclitaxel and concurrent radiation therapy for locally advanced non-small cell lung cancer. *Clin Cancer Res* **4:** 1931–1936

Cividalli A, Arcangeli G, Cruciani G, Livdi E, Cordelli E, Danesi DT (1998) Enhancement of radiation response by paclitaxel in mice according to different treatment schedules. *Int J Radiat Oncol Biol Phys* **40:** 1163–1170

Dillman RO, Seagren SL, Propert KJ, Guerra J, Eaton WL, Perry MC, Carey RW, Frei III EF, Green MR (1990) A randomized trial of induction

chemotherapy plus high-dose radiation *vs* radiation alone in stage III non-small-cell lung cancer. *N Engl J Med* **323:** 940–945

Dowell JE, Sinard R, Yardley DA, Aviles V, Machtay M, Weber RS, Weinstein GS, Chalian AA, Carbone DP, Rosenthal DI (1999) Seven-week continuous-infusion paclitaxel concurrent with radiation therapy for locally advanced non-small cell lung and head and neck cancers. *Semin Radiat Oncol* **9:** 97–101

Early Breast Cancer Trialists' Collaborative Group (2000) Favourable and unfavourable effects on long-term survival of radiotherapy for early breast cancer: an overview of the randomised trials. Early Breast Cancer Trialists' Collaborative Group. *Lancet* **355:** 1757–1770

Ellerbroek N, Martino S, Mautner B, Tao ML, Rose C, Botnick L (2003) Breast-conserving therapy with adjuvant paclitaxel and radiation therapy: feasibility of concurrent treatment. *Breast J* **9:** 74–78

Formenti SC, Volm M, Skinner KA, Spicer D, Cohen D, Perez E, Bettini AC, Groshen S, Gee C, Florentine B, Press M, Danenberg P, Muggia F (2003) Preoperative twice-weekly paclitaxel with concurrent radiation therapy followed by surgery and postoperative doxorubicin-based chemotherapy in locally advanced breast cancer: a phase I/II trial. *J Clin Oncol* **21:** 864–870

Furuse K, Fukuoka M, Kawahara M, Nishikawa H, Takada Y, Kudoh S, Katagami N, Ariyoshi Y (1999) Phase III study of concurrent *vs* sequential thoracic radiotherapy in combination with mitomycin, vindesine, and cisplatin in unresectable stage III non-small-cell lung cancer. *J Clin Oncol* **17:** 2692–2699

Gabizon A, Chemla M, Tzemach D, Horowitz AT, Goren D (1996) Liposome longevity and stability in circulation: effects on the *in vivo* delivery to tumors and therapeutic efficacy of encapsulated anthracyclines. *J Drug Target* **3:** 391–398

Hamaguchi T, Matsumura Y, Suzuki M, Shimizu K, Goda R, Nakamura I, Nakatomi I, Yokoyama M, Kataoka K, Kakizoe T (2005) NK105, a paclitaxel-incorporating micellar nanoparticle formulation, can extend *in vivo* antitumour activity and reduce the neurotoxicity of paclitaxel. *Br J Cancer* **92:** 1240–1246

Hanna YM, Baglan KL, Stromberg JS, Vicini FA, A Decker D (2002) Acute and subacute toxicity associated with concurrent adjuvant radiation therapy and paclitaxel in primary breast cancer therapy. *Breast J* **8:** 149–153

Kao J, Conzen SD, Jaskowiak NT, Song DH, Recant W, Singh R, Masters GA, Fleming GF, Heimann R (2005) Concomitant radiation therapy and paclitaxel for unresectable locally advanced breast cancer: results from two consecutive phase I/II trials. *Int J Radiat Oncol Biol Phys* **61:** 1045–1053

Khayat D, Antoine EC, Coeffic D (2000) Taxol in the management of cancers of the breast and the ovary. *Cancer Invest* **18:** 242–260

Klibanov AL, Maruyama K, Beckerleg AM, Torchilin VP, Huang L (1991) Activity of amphipathic poly(ethylene glycol) 5000 to prolong the circulation time of liposomes depends on the liposome size and is unfavorable for immunoliposome binding to target. *Biochim Biophys Acta* **1062:** 142–148

Klibanov AL, Maruyama K, Torchilin VP, Huang L (1990) Amphipathic polyethyleneglycols effectively prolong the circulation time of liposomes. *FEBS Lett* **268:** 235–237

Lind PA, Marks LB, Hardenbergh PH, Clough R, Fan M, Hollis D, Hernando ML, Lucas D, Piepgrass A, Prosnitz LR (2002) Technical factors associated with radiation pneumonitis after local +/− regional radiation therapy for breast cancer. *Int J Radiat Oncol Biol Phys* **52:** 137–143

Lokeshwar BL, Ferrell SM, Block NL (1995) Enhancement of radiation response of prostatic carcinoma by taxol: therapeutic potential for late-stage malignancy. *Anticancer Res* **15:** 93–98

Maeda H, Matsumura Y (1989) Tumoritropic and lymphotropic principles of macromolecular drugs. *Crit Rev Ther Drug Carrier Syst* **6:** 193–210

Mason KA, Milas L, Peters LJ (1995) Effect of paclitaxel (taxol) alone and in combination with radiation on the gastrointestinal mucosa. *Int J Radiat Oncol Biol Phys* **32:** 1381–1389

Matsumura Y, Maeda H (1986) A new concept for macromolecular therapeutics in cancer chemotherapy: mechanism of tumoritropic accumulation of proteins and the antitumor agent smancs. *Cancer Res* **46:** 6387–6392

Milas L, Hunter NR, Mason KA, Kurdoglu B, Peters LJ (1994) Enhancement of tumour radioresponse of a murine mammary carcinoma by paclitaxel. *Cancer Res* **54:** 3506–3510

Milas L, Hunter NR, Mason KA, Milross CG, Saito Y, Peters LJ (1995) Role of reoxygenation in induction of enhancement of tumour radioresponse by paclitaxel. *Cancer Res* **55:** 3564–3568

Morton RF, Jett JR, McGinnis WL, Earle JD, Therneau TM, Krook JE, Elliott TE, Mailliard JA, Nelimark RA, Maksymiuk AW (1991) Thoracic radiation therapy alone compared with combined chemoradiotherapy for locally unresectable non-small cell lung cancer. A randomized, phase III trial. *Ann Intern Med* **115:** 681–686

Penney DP, Rubin P (1977) Specific early fine structural changes in the lung irradiation. *Int J Radiat Oncol Biol Phys* **2:** 1123–1132

Rodriguez M, Sevin BU, Perras J, Nguyen HN, Pham C, Steren AJ, Koechli OR, Averette HE (1995) Paclitaxel: a radiation sensitizer of human cervical cancer cells. *Gynecol Oncol* **57:** 165–169

Rowinsky EK, Chaudhry V, Forastiere AA, Sartorius SE, Ettinger DS, Grochow LB, Lubejko BG, Cornblath DR, Donehower RC (1993) Phase I and pharmacologic study of paclitaxel and cisplatin with granulocyte colony-stimulating factor: neuromuscular toxicity is dose-limiting. *J Clin Oncol* **11:** 2010–2020

Rowinsky EK, Donehower RC (1995) Paclitaxel (taxol). *N Engl J Med* **332:** 1004–1014

Sause W, Kolesar P, Taylor SI, Johnson D, Livingston R, Komaki R, Emami B, Curran Jr W, Byhardt R, Dar AR, Turrisi III A (2000) Final results of phase III trial in regionally advanced unresectable non-small cell lung cancer: Radiation Therapy Oncology Group, Eastern Cooperative Oncology Group, and Southwest Oncology Group. *Chest* **117:** 358–364

Sinclair WK, Morton RA (1966) X-ray sensitivity during the cell generation cycle of cultured Chinese hamster cells. *Radiat Res* **29:** 450–474

Taghian AG, Assaad SI, Niemierko A, Kuter I, Younger J, Schoenthaler R, Roche M, Powell SN (2001) Risk of pneumonitis in breast cancer patients treated with radiation therapy and combination chemotherapy with paclitaxel. *J Natl Cancer Inst* **93:** 1806–1811

Terasima T, Tolmach LJ (1963) X-ray sensitivity and DNA synthesis in synchronous populations of HeLa cells. *Science* **140:** 490–492

Tishler RB, Geard CR, Hall EJ, Schiff PB (1992) Taxol sensitizes human astrocytoma cells to radiation. *Cancer Res* **52:** 3495–3497

Uchino H, Matsumura Y, Negishi T, Koizumi F, Hayashi T, Honda T, Nishiyama N, Kataoka K, Naito S, Kakizoe T (2005) Cisplatin-incorporating polymeric micelles (NC-6004) can reduce nephrotoxicity and neurotoxicity of cisplatin in rats. *Br J Cancer* **93:** 678–687

Weiss RB, Donehower RC, Wiernik PH, Ohnuma T, Gralla RJ, Trump DL, Baker Jr JR, Van Echo DA, Von Hoff DD, Leyland-Jones B (1990) Hypersensitivity reactions from taxol. *J Clin Oncol* **8:** 1263–1268

Yu TK, Whitman GJ, Thames HD, Strom E, McNeese MD, Perkins GH, Schechter N, Kau S, Buzdar AU, Hortobagyi GN, Thomas E, Buchholz TA (2003) Clinically-relevant pneumonitis is not increased in breast cancer patients treated with sequential paclitaxel and radiation. *Int J Radiat Oncol Biol Phys* **57**(2 Suppl): S127–S128

Yu TK, Whitman GJ, Thames HD, Buzdar AU, Strom EA, Perkins GH, Schechter NR, McNeese MD, Kau SW, Thomas ES, Hortobagyi GN, Buchholz TA (2004) Clinically relevant pneumonitis after sequential paclitaxel-based chemotherapy and radiotherapy in breast cancer patients. *J Natl Cancer Inst* **96:** 1676–1681

Novel SN-38–Incorporating Polymeric Micelles, NK012, Eradicate Vascular Endothelial Growth Factor–Secreting Bulky Tumors

Fumiaki Koizumi,[1] Masayuki Kitagawa,[2] Takahito Negishi,[1] Takeshi Onda,[2] Shin-ichi Matsumoto,[2] Tetsuya Hamaguchi,[3] and Yasuhiro Matsumura[1]

[1]Investigative Treatment Division, Research Center for Innovative Oncology, National Cancer Center Hospital East, Kashiwa, Chiba, Japan; [2]Pharmaceutical Research Laboratories, Research and Development Group, Nippon Kayaku Co., Ltd, Kita-ku, Tokyo, Japan; and [3]Department of Medicine, National Cancer Center Hospital, Tyuo-ku, Tokyo, Japan

Abstract

7-Ethyl-10-hydroxy-camptothecin (SN-38), a biological active metabolite of irinotecan hydrochloride (CPT-11), has potent antitumor activity but has not been used clinically because it is a water-insoluble drug. For delivery by i.v. injection, we have successfully developed NK012, a SN-38-releasing nanodevice. The purpose of this study is to investigate the pharmacologic character of NK012 as an anticancer agent, especially in a vascular endothelial growth factor (VEGF)–secreting tumor model. The particle size of NK012 was ~20 nm with a narrow size distribution. NK012 exhibited a much higher cytotoxic effect against lung and colon cancer cell lines as compared with CPT-11. NK012 showed significantly potent antitumor activity against a human colorectal cancer HT-29 xenograft as compared with CPT-11. Enhanced and prolonged distribution of free SN-38 in the tumor was observed after the injection of NK012. NK012 also had significant antitumor activity against bulky SBC-3/Neo (1,533.1 ± 1,204.7 mm^3) and SBC-3/VEGF tumors (1,620.7 ± 834.0 mm^3) compared with CPT-11. Furthermore, NK012 eradicated bulky SBC-3/VEGF tumors in all mice but did not eradicate SBC-3/Neo tumors. In the drug distribution analysis, an increased accumulation of SN-38 in SBC-3/VEGF tumors was observed as compared with that in SBC-3/Neo tumors. NK012 markedly enhanced the antitumor activity of SN-38, especially in highly VEGF-secreting tumors, and could be a promising SN-38-based formulation. (Cancer Res 2006; 66(20): 10048-56)

Introduction

The antitumor plant alkaloid camptothecin (CPT) is a broad-spectrum anticancer agent that targets DNA topoisomerase I. Although CPT has shown promising antitumor activity *in vitro* and *in vivo* (1, 2), it has not been clinically used because of its low therapeutic efficacy and severe toxicity (3, 4). Among CPT analogues, irinotecan hydrochloride (CPT-11) has recently been shown to be active against colorectal, lung, and ovarian cancer (5–9). CPT-11 itself is a prodrug and is converted to 7-ethyl-10-hydroxy-CPT (SN-38), a biologically active metabolite of CPT-11, by carboxylesterases. SN-38 exhibits up to 1,000-fold more potent cytotoxic activity against various cancer cells *in vitro* than CPT-11 (10). Although CPT-11 is converted to SN-38 in the liver and tumor, the metabolic conversion rate is <10% of the original volume of CPT-11 (11, 12). In addition, the conversion of CPT-11 to SN-38 depends on the genetic interindividual variability of carboxylesterase activity (13). Thus, direct use of SN-38 might be of great advantage and attractive for cancer treatment. For the clinical use of SN-38, however, it is essential to develop a soluble form of water-insoluble SN-38. The progress of the manufacturing technology of "micellar nanoparticles" may make it possible to use SN-38 for *in vivo* experiments and further clinical use.

Passive targeting of drug delivery system is based on the pathophysiologic characteristics that are observed in many solid tumors: hypervascularity, irregular vascular architecture, potential for secretion of vascular permeability factors, and the absence of effective lymphatic drainage that prevents efficient clearance of macromolecules. These characteristics, unique to solid tumors, are believed to be the basis of the enhanced permeability and retention effect (14–17). Supramolecular structures, such as liposomes and polymeric micelles, are expected to increase the accumulation of drugs in tumor tissue through these pathophysiologic features. Polymeric micelle–based anticancer drugs have been developed in recent years (18–20), and some of them have been under evaluation for clinical trials (21–23). This carrier system can incorporate various kinds of drugs into the inner core by chemical conjugation or physical entrapment with relatively high stability, and the size can be controlled within the range of 20 to 100 nm in diameter. This range of diameters is too large to pass through normal vessel walls; therefore, the drug can be expected to reduce side effects due to a decrease in volume of distribution.

Angiogenesis is essential for the growth and metastasis of solid tumors (24). The clinical importance of angiogenesis in human tumors was shown by several reports indicating a positive relationship between the blood vessel density in the tumor mass and poor prognosis for survival in patients with various types of cancers (25–28). Furthermore, Natsume et al. (29) reported that the antitumor activities of anticancer agents, including *cis*-diammine-dichloroplatinum, vincristine, and docetaxel, were less active against vascular endothelial growth factor (VEGF)–secreting cells, SBC-3/VEGF, *in vivo* as compared with its mock transfectant (SBC-3/Neo), although the high vascularity should have been favorable for the drug delivery.

VEGF is also well known as a potent vascular permeability factor (30). The ability of supramolecular structures to accumulate in target tissue is based on the enhanced tumor angiogenesis and tumor vascular permeability that occur in solid tumors. Therefore, we hypothesized that a polymeric micelle–based drug carrier would increase its accumulation and deliver enhanced therapeutic efficacy in tumors that secrete higher levels of VEGF. In the present study, we present the superiority of NK012 over CPT-11 in a tumor model,

Requests for reprints: Yasuhiro Matsumura, Investigative Treatment Division, Research Center for Innovative Oncology, National Cancer Center Hospital East, 6-5-1 Kashiwanoha, Kashiwa, Chiba 277-8577, Japan. Phone: 81-4-7134-6857; Fax: 81-4-7134-6857; E-mail: yhmatsum@east.ncc.go.jp.

doi:10.1158/0008-5472.CAN-06-1605

especially in a VEGF-secreting tumor, and we illustrate the outstanding advantage of polymeric micelle–based drug carriers.

Materials and Methods

Drugs and Cells

SN-38 was synthesized by Nippon Kayaku Co., Ltd. (Tokyo, Japan). CPT-11 was purchased from Yakult Honsha Co., Ltd. (Tokyo, Japan). Human colon cancer cell lines WiDR, SW480, Lovo, and HT-29 and human non–small-cell lung cancer cell line A431 were purchased from American Type Culture Collection (Rockville, MD). Human small-cell lung cancer cell line SBC-3 and human non–small-cell lung cancer cell line PC-14 were kindly provided by Dr. I. Kimura (Okayama University, Okayama, Japan) and Dr. Y. Hayata (Tokyo Medical University, Tokyo, Japan), respectively. SBC-3 and PC-14 were maintained in RPMI 1640 supplemented with 10% fetal bovine serum (Cell Culture Technologies, Gaggenau-Hoerden, Germany), penicillin, streptomycin, and amphotericin B (100 units/mL, 100 μg/mL, and 25 μg/mL, respectively; Sigma, St. Louis, MO) in a humidified atmosphere of 5% CO_2 at 37°C. Other cell lines were maintained in DMEM (Nikken Bio Med. Lab., Kyoto, Japan) supplemented with 10% fetal bovine serum. SBC-3/Neo and SBC-3/VEGF were generated from SBC-3 cells that were transfected with BMG-Neo and BMG-Neo-VEGF as previously reported (29). The full-length sequence of human VEGF expressing 206 amino acids (31) was selected. SBC-3/VEGF cells express ~100 times more soluble VEGF than SBC-3/Neo and SBC-3 cells in the supernatant of cultured cells as shown by ELISA (29).

Preparation of an SN-38–Conjugated Poly(Ethylene Glycol)-Poly(Glutamic Acid) Block Copolymer for NK012 Construction

Poly(ethylene glycol)-poly(glutamic acid) block copolymer [PEG-PGlu(SN-38)] was synthesized as follows: A poly(ethylene glycol)-poly(glutamic acid) block copolymer [PEG-PGlu] was prepared according to the previously reported technique (32, 33). SN-38 was covalently introduced into the PGlu segment by the condensation reaction between the carboxylic acid on PGlu and the phenol on SN-38 with 1,3-diisopropylcarbodiimide and *N,N*-dimethylaminopyridine at 26°C. Consequently, the PGlu segment obtained sufficient hydrophobicity. Accordingly, NK012 was constructed with self-assembling PEG-PGlu(SN-38) amphiphilic block copolymers in an aqueous milieu.

Determination of the Size Distribution of NK012 and Drug Release Behavior of SN-38 from NK012

The size distribution of NK012 was measured with the dynamic light scattering method at 25°C using a Particle Sizer NICOMP 380ZLS (Particle Sizing Systems, Santa Barbara, CA). The release behavior of SN-38 from NK012 was investigated *in vitro* at 20°C or 37°C in PBS (pH 7.3) or 5% glucose solution (pH 4.6). The concentration was 0.1 mg/mL. The amount of SN-38 released from NK012 was estimated by UV measurement at 265 nm.

In vitro Growth Inhibition Assay

The growth inhibitory effects of NK012, SN-38, and CPT-11 were examined with a 3-(4,5-dimethylthiazol-2-yl)-2,5-diphenyltetrazolium bromide (MTT) assay. One hundred eighty microliters of an exponentially growing cell suspension (6×10^3/mL-12×10^3/mL) were seeded into a 96-well microtiter plate, and 20 μL of various concentrations of each drug were added. After incubation for 72 hours at 37°C, 20 μL of MTT solution (5 mg/mL in PBS) were added to each well and the plates were incubated for an additional 4 hours at 37°C. After centrifuging the plates at 200 × *g* for 5 minutes, the medium was aspirated from each well, and 180 μL of DMSO were added to each well to dissolve the formazan. The growth inhibitory effect of each drug was assessed spectrophotometrically (SpectraMax 190, Molecular Devices Corp., Sunnyvale, CA).

In vivo Growth Inhibition Assay

The animal experimental protocols were approved by the Committee for Ethics of Animal Experimentation and the experiments were conducted in accordance with the Guidelines for Animal Experiments in the National Cancer Center or Nippon Kayaku.

Experiment 1. Female BALB/c nude mice, 7 weeks old, were purchased from CLEA Japan (Tokyo, Japan). Human colorectal cancer HT-29 cells were grown as s.c. tumor in the flank of the mice. The tumors were excised from the mice and fragments were inoculated s.c. in the mouse flank. When the tumor volume reached 70 to 170 mm^3, mice were randomly divided into test groups consisting of six mice per group (day 0). Drugs were administered on days 0, 4, and 8 by i.v. injection into the tail vein. NK012 was given at doses of 30 (maximum tolerated dose), 15, and 7.5 mg/kg/d. The reference drug, CPT-11, was given at the maximum tolerated dose, 66.7 mg/kg/d, in the optimal schedule reported (34). The length (a) and width (b) of the tumor mass were measured twice a week, and the tumor volume (TV) was calculated as follows: $TV = (a \times b^2) / 2$. Relative tumor volumes at day n were calculated according to the following formula: $RTV = TV_n / TV_0$, where TV_n is the tumor volume at day n, and TV_0 is the tumor volume at day 0. Differences in relative tumor sizes between the treatment groups at day 21 were analyzed with an unpaired t test.

Experiment 2. As a hypervascular tumor model, we used SBC-3/VEGF cells. SBC-3/Neo or SBC-3/VEGF cells (10^7) were s.c. injected into the back of mice. NK012 or CPT-11 was administered when the mean tumor volumes ($n = 4$) reached a massive size of 1,500 mm^3, which gave tumors almost 1.5 cm in length. It took ~65 days for SBC-3/Neo and 20 days for SBC-3/VEGF to reach the tumor volume of 1,500 mm^3 from the day of inoculation. NK012 at a dose of 10 or 20 mg/kg/d and CPT-11 at a dose of 15 or 30 mg/kg/d were administered i.v. on days 0, 4, and 8. Differences in tumor sizes between the treatment groups and control group at day 14 were analyzed with an unpaired t test.

Histologic and Immunohistochemical Analysis

Histologic sections were taken from SBC-3/Neo and SBC-3/VEGF tumor tissues when the volumes reached 1,500 mm^3. After extirpation, tissues were fixed with 3.9% formalin in PBS (pH 7.4), and the subsequent preparations and H&E staining were done by Tokyo Histopathologic Laboratory Co., Ltd. (Tokyo, Japan). For detection of tumor blood vessels, polyclonal anti–von Willebrand factor antibody (Dako, Glostrup, Denmark) was used.

Assay for SN-38 and CPT-11 in Plasma and Tissues

Female BALB/c nude mice bearing HT-29 (as mentioned in experiment 1; $n = 3$) were used for the analysis of the biodistribution of NK012 and CPT-11. NK012 (30 mg/kg) or CPT-11 (66.7 mg/kg) was administered i.v. to the mice. Under anesthesia, blood and tumor samples were taken at 5 minutes, 1, 6, 24, 48, 72, and 168 hours after administration of NK012 and at 5 minutes, 1, 3, 6, and 24 hours after administration of CPT-11. The blood samples were collected in microtubes and immediately centrifuged at 1,600 × *g* for 15 minutes. The plasma and tumor samples were stored at −80°C until analysis.

For the biodistribution study in hypervascular tumors (experiment 2), female BALB/c nude mice ($n = 3$) bearing 1,500-mm^3 massive SBC-3/Neo and SBC-3/VEGF tumors were used. NK012 (20 mg/kg) and CPT-11 (30 mg/kg) were administered on day 0. The mice were sacrificed at 1, 6, 24, and 72 hours (day 3) after administration. The tumor, liver, spleen, upper small intestine, lung, and blood were taken and stored at −80°C until analysis.

Preparation of the free SN-38 (polymer-unbound SN-38) and CPT-11. Tumor samples were homogenized on ice using a Digital homogenizer (Iuchi, Osaka, Japan) and suspended in the mixture of 100 mmol/L glycine-HCl buffer (pH 3)/methanol (1:1, v/v) at a concentration of 5% w/w. The concentrations of free SN-38 and CPT-11 in the plasma and tumor from aliquots of the homogenates (100 μL) and plasma (50 μL) were determined by high-performance liquid chromatography. For free SN-38 (polymer-unbound SN-38) and CPT-11, proteins were precipitated with an ice-cold mixture of methanol/H_2O/$HClO_4$ (50:45:5, v/v/v) containing CPT as an internal standard. The sample was vortexed for 10 seconds, filtered through a MultiScreen Solvinert (Millipore Corp., Bedford, MA), and analyzed.

Preparation of the polymer-bound SN-38 (SN-38 remaining bound to PEG-PGlu). To permit complete release of SN-38 from the conjugate, 20 μL of plasma and 100 μL of tissue samples were diluted with 20 μL of methanol (50%, v/v) and 20 μL of NaOH (0.3 mol/L for plasma and 0.7 mol/L for tissue). The samples were incubated for 15 minutes at 25°C. After incubation, 20 μL of HCl (0.3 mol/L for plasma and 0.7 mol/L for tissue) and 60 μL of internal standard solution were added to the samples, and then the hydrolysis was filtered through a MultiScreen Solvinert. The filtrate was applied to the high-performance liquid chromatography system.

High-performance liquid chromatography. Reversed-phase high-performance liquid chromatography was done at 35°C on a Mightysil RP-18 GP column 150 × 4.6 mm (Kanto Chemical Co., Inc., Tokyo, Japan). The samples were injected into an Alliance Waters 2795 high-performance liquid chromatography system (Waters, Milford, MA) equipped with a Waters 2475 multi λ fluorescence detector. The detector was set at 365 and 430 nm (excitation and emission, respectively) for CPT-11 and CPT, and at 365 and 540 nm for SN-38. A reversed-phase column was used at 35°C. The mobile phase was a mixture of 100 mmol/L ammonium acetate (pH 4.2) and methanol [11:9 (v/v) for SN-38 in plasma and tumor, 3:2 (v/v) for CPT-11 in plasma, and 63:37 (v/v) for CPT-11 in tumor]. The flow rate was 1.0 mL/min. Peak data were recorded with a chromatography management system (Empower, Waters). Polymer-bound SN-38 was determined by subtraction of polymer-unbound SN-38 from the total SN-38 of the hydrolysate.

Pharmacokinetic and Statistical Analyses

The concentrations of SN-38 and CPT-11 in plasma and tissue were fitted to a pharmacokinetic model by the nonlinear least-square method using WinNonlin Professional software (version 4.1; Pharsight Corp., Palo Alto, CA). We used a noncompartmental analysis. The pharmacokinetic variables were calculated using the following equations (AUC_{last} was calculated by the trapezoidal rule to the last measurable data point):

$$AUC_{inf.} = \int_0^{\infty} C(t)dt$$

$$T_{1/2z}(\text{terminal half} - \text{life}) = 0.693/\lambda z$$

(λz is first-order rate constant associated with the terminal portion of the curve)

$$CL_{tot} = \text{Dose}/AUC_{inf.}$$

$$V_{ss} = \text{MRT} \times CL_{tot}(\text{MRT}, \text{mean residence time})$$

Data were expressed as mean ± SD. Data were analyzed with the Student's t test when the groups showed equal variances (F test) or with Welch's test when they showed unequal variances (F test). $P < 0.05$ was regarded as statistically significant. All statistical tests were two sided.

Results

Preparation and characterization of NK012. NK012 is an SN-38-loaded polymeric micelle constructed in an aqueous milieu by the self-assembly of an amphiphilic block copolymers, PEG-PGlu(SN-38). The molecular weight of PEG-PGlu(SN-38) was determined to be ~19,000 (PEG segment, 12,000; SN-38-conjugated PGlu segment, 7,000). NK012 was obtained as a freeze-dried formulation and contained ca. 20% (w/w) of SN-38 (Fig. 1*A*). The mean particle size of NK012 is 20 nm in diameter with a relatively narrow range (Fig. 1*B*). The releasing rates of SN-38 from NK012 in PBS at 37°C were 57% and 74% at 24 and 48 hours, respectively, and those in 5% glucose solution at 37°C were 1% and 3% at 24 and 48 hours, respectively (Fig. 1*C*). SN-38 is loaded by chemical bonding to the block copolymer. The bonding is phenyl ester bond, which is stable under acidic condition and labile under mild alkaline condition. These results indicate that NK012 can release SN-38 under neutral condition even without the presence of a hydrolytic enzyme and is stable in 5% glucose solution. It is suggested that NK012 is stable before administration and starts to release SN-38, the active component, under physiologic conditions after administration.

Cellular sensitivity of non–small-cell lung cancer and colon cancer cells to SN-38, NK012, and CPT-11. The IC_{50} values of NK012 for the cell lines ranged from 0.009 μmol/L (SBC-3 cells) to 0.16 μmol/L (WiDR cells). The growth inhibitory effects of NK012 are 43- to 340-fold more potent than those of CPT-11, whereas the IC_{50} values of NK012 were 2.3- to 5.8-fold higher than those of SN-38. NK012 exhibited a higher cytotoxic effect against each cell line as compared with CPT-11 (43- to 340-fold sensitivity). On the other hand, the IC_{50} values of NK012 were a little higher than those of SN-38, similar to the cytotoxic feature also reported in a previous study about micellar drugs (ref. 23; Table 1).

Antitumor activity and pharmacokinetic analysis of NK012 and CPT-11 using HT-29–bearing nude mice (experiment 1). Potent activity was observed in mice treated with NK012 at doses of 15 and 30 mg/kg (Fig. 2*A*), although neither CPT-11 at a dose of 66.7 mg/kg/d nor NK012 at a dose of 7.5 mg/kg/d exerted any significant antitumor activity *in vivo*. Comparison of the relative tumor volume at day 21 revealed significant differences between 15 mg/kg/d NK012 and 66.7 mg/kg/d CPT-11 and between 30 mg/kg/d NK012 and 66.7 mg/kg/d CPT-11 ($P < 0.05$). Although treatment-related body weight loss was observed in mice treated with each drug, body weight recovered by day 21 (Fig. 2*B*). These results clearly show the significant *in vivo* activity of NK012 against HT-29.

After injection of CPT-11, the concentrations of CPT-11 and SN-38 for plasma declined rapidly with time in a log-linear fashion. On the other hand, NK012 (polymer-bound SN-38) exhibited slower clearance (Fig. 3*A*). The clearance of NK012 in the HT-29 tumor was significantly slower and the concentration of free SN-38 was maintained at >30 ng/g even at 168 hours after injection (Fig. 3*B*). The pharmacokinetic variables of each drug in the plasma and tumor are depicted in Table 2.

Tumor-to-plasma concentration ratios (Kp) of polymer-bound and free SN-38 increased during the observation period. The highest value of Kp was achieved at 168 hours after administration, 108 for polymer-bound and 11.0 for free SN-38 (Table 3). These results indicate that NK012 can remain in the tumor tissue for a longer period and release free SN-38.

Antitumor activity and the distribution of NK012 and CPT-11 in SBC-3/Neo or SBC-3/VEGF tumors (experiment 2). To determine whether the potent antitumor effect of NK012 is enhanced in the tumors with high vascularity, we used VEGF-secreting cells SBC-3/VEGF. There was no significant difference in the *in vitro* cytotoxic activity of each drug between SBC-3/Neo and SBC-3/VEGF (Fig. 4*A*). SBC-3/VEGF tumors are reddish by gross evaluation as compared with SBC-3/Neo tumors (Fig. 4*B*). Histologic and immunohistochemical (von Willebrand factor) examination revealed that prominent leakage of erythrocytes and high vascularity were observed in SBC-3/VEGF tumor xenografts. On the other hand, SBC-3/Neo tumors have less tumor vasculatures and more interstitial space as compared with SBC-3/VEGF tumors

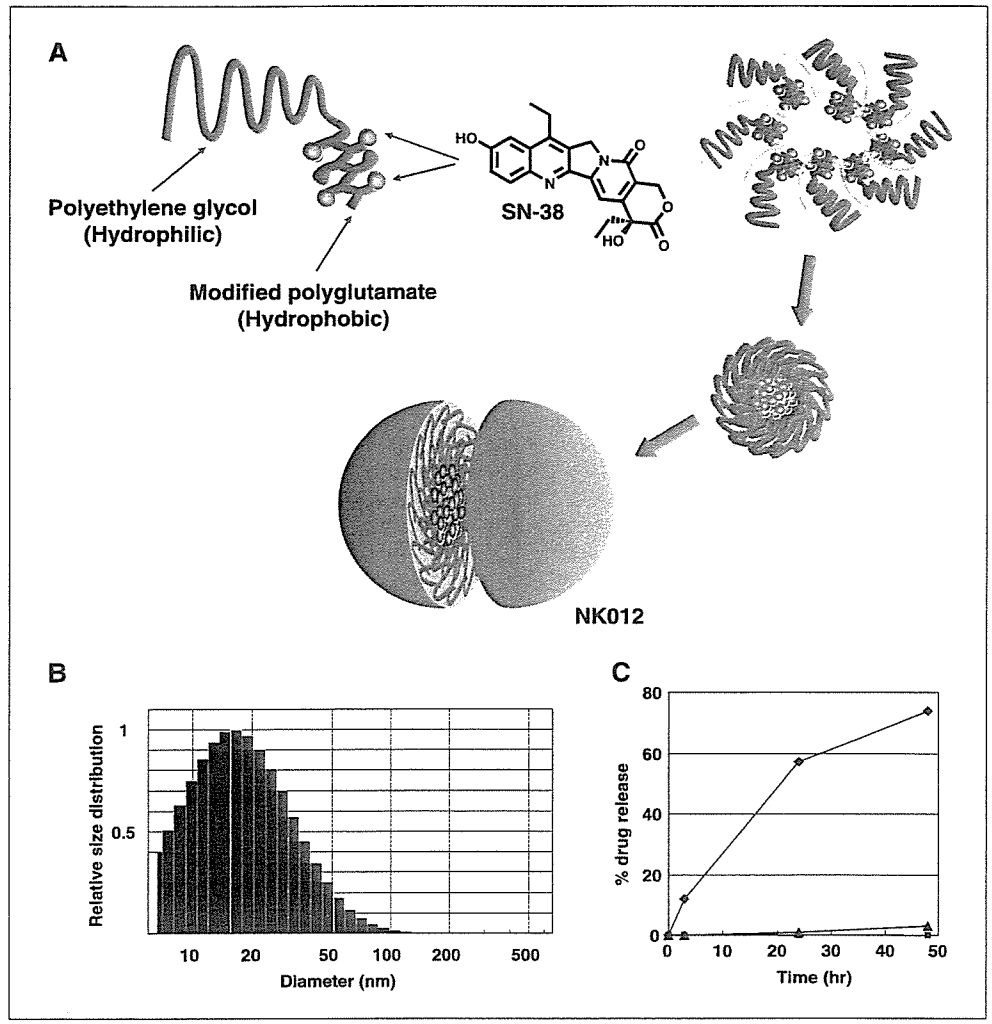

Figure 1. Preparation and characterization of NK012. *A*, schematic structure of NK012. A polymeric micelle carrier of NK012 consists of a block copolymer of PEG (molecular weight of ~12,000) and partially modified polyglutamate (~20 units). PEG (hydrophilic) is believed to be the outer shell and SN-38 was incorporated into the inner core of the micelle. *B*, size distribution of NK012 measured with the dynamic light scattering method. The *Y* axis shows relative particle size distribution. *C*, release of free SN-38 from the micelles in PBS [pH 7.3, 37°C (◆)] or 5% glucose solution [pH 4.6, 20°C (■), 37°C (▲)].

(Fig. 4*B*). Deviating from the ordinary experimental tumor model, tumors were allowed to grow until they became massive in size, ~1.5 cm (Fig. 4*C*), and then the treatment was initiated. NK012 at doses of 15 and 30 mg/kg showed potent antitumor activity against bulky SBC-3/Neo tumors (1,533.1 ± 1,204.7 mm^3) as compared with CPT-11 (Fig. 4*C*). Striking antitumor activity was observed in mice treated with NK012 (Fig. 4*C*) when we compared the antitumor activity of NK012 with that of CPT-11 using SBC-3/VEGF cells. SBC-3/VEGF bulky masses (1,620.7 ± 834.0 mm^3) disappeared in all mice, although relapse 3 months after treatment was noted in one mouse treated with NK012 20 mg/kg. On the other hand, SBC-3/VEGF were not eradicated and rapidly regrew after a partial response in mice treated with CPT-11. Approximately 10% body weight loss was observed in mice treated with 20 mg/kg NK012, but no significant difference was observed in comparison with mice treated with 30 mg/kg CPT-11.

We then examined the distribution of free SN-38 in the SBC-3/Neo and SBC-3/VEGF masses after administration of NK012 and CPT-11. In the case of CPT-11 administration, the concentrations at 1 and 6 hours after the administration were <100 ng/g both in the SBC-3/Neo and SBC-3/VEGF tumors and were almost negligible at 24 hours in both tumors (Fig. 5*A*). There was no significant difference in the concentration between the SBC-3/Neo and SBC-3/VEGF tumors. On the other hand, in the case of NK012 administration, free SN-38 was detectable in the tumors even at 72 hours after the administration. The concentrations of free SN-38 were higher in the SBC-3/VEGF tumors than those in the SBC-3/Neo tumors at any time point during the period of observation (significant at 1, 6, and 24 hours; $P < 0.05$; Fig. 5*A*).

Tissue distribution of SN-38 after administration of NK012 and CPT-11. We examined the concentration-time profile of free SN-38 in various tissues after i.v. administration of NK012 and

Table 1. *In vitro* growth inhibitory activity of SN-38, NK012, and CPT-11 in human lung and colorectal cancer cells (MTT assay)

Cell line	IC_{50} (μmol/L)		
	SN-38	NK012	CPT-11
WiDR	0.046 ± 0.008	0.16 ± 0.014	20.4 ± 1.6
SW480	0.025 ± 0.003	0.11 ± 0.028	31.9 ± 1.3
Lovo	0.0067 ± 0.0012	0.026 ± 0.003	7.24 ± 1.04
HT-29	0.016 ± 0.003	0.068 ± 0.007	23.1 ± 2.63
PC-14	0.044 ± 0.025	0.14 ± 0.021	5.96 ± 0.90
SBC-3	0.0016 ± 0.001	0.0093 ± 0.005	0.72 ± 0.22
A431	0.0081 ± 0.002	0.019 ± 0.007	5.6 ± 1.5

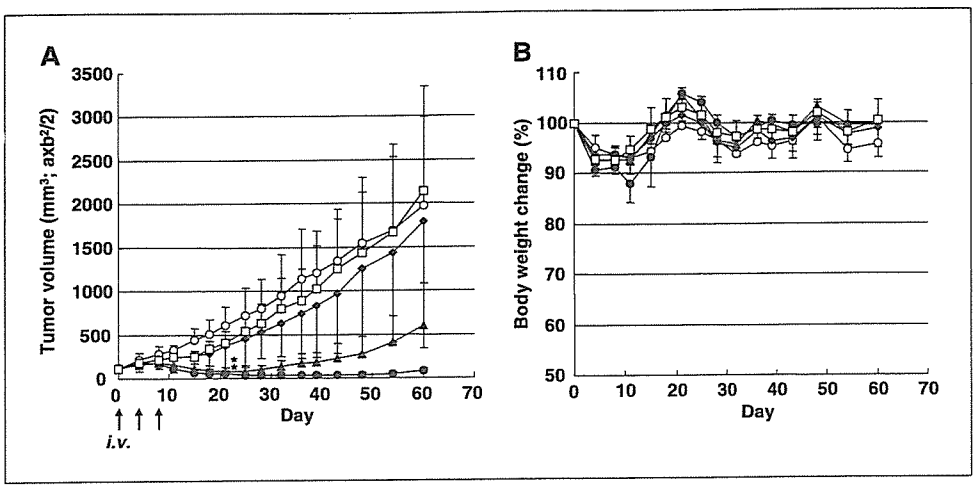

Figure 2. The effect of NK012 and CPT-11 against an HT-29 tumor xenograft. *A*, HT-29 tumor was inoculated s.c. into the flank of mice as described in Materials and Methods. CPT-11 at a dose of 66.7 mg/kg/d (□), NK012 at a dose of 7.5 mg/kg/d (◆), NK012 at a dose of 15 mg/kg/d (▲), or NK012 at a dose of 30 mg/kg/d (●) was administered i.v. on days 0, 4, and 8 (○, no treatment). Tumor volume in mice treated with CPT-11 or NK012. *Points*, mean; *bars*, SD. *, $P < 0.05$. *B*, treatment-related body weight loss occurred in mice treated with CPT-11 and NK012. *Points*, mean; *bars*, SD.

CPT-11. All organs measured exhibited the highest concentration of SN-38 at 1 hour after administration in mice given CPT-11 (Fig. 5*B*). On the other hand, mice given NK012 exhibited prolonged distribution in the liver and spleen (Fig. 5*B*). In a similar manner to other micellar drugs (19, 23), NK012 showed relatively higher accumulation in organs of the reticuloendothelial system. In the lung, kidney, and small intestine, the highest concentration of free SN-38 was achieved at 1 hour after injection of NK012 and the concentration was almost negligible at 24 hours. Although relatively high at 1 hour after administration of NK012 and CPT-11, the concentrations of free SN-38 in the small intestine rapidly decreased. Interestingly, there was no significant difference in the kinetic character of free SN-38 in the small intestine between mice treated with NK012 and CPT-11.

Discussion

The drug-incorporating polymeric micelle has characteristic pharmacokinetic features. These structures are too large to pass through normal vessel walls and evade renal excretion. The outer shell of the drug with PEG diminishes nonspecific capture by the reticuloendothelial system. Therefore, the drug can be expected to achieve a long half-life, which permits a large amount of the drug-incorporating micelles to reach the tumor site through the enhanced permeability and retention effect. The pharmacokinetic study revealed that the plasma AUC of polymer-bound SN-38 after administration of NK012 at a dose of 30 mg/kg to the HT-29-bearing mice was ~200-fold higher than that of CPT-11 at a dose of 66.7 mg/kg. A 14-fold higher AUC of the free SN-38 was achieved in mice given NK012 compared with mice given CPT-11. Prolonged circulation of NK012 in the blood might increase the accumulation of NK012 in a tumor tissue due to the enhanced permeability and retention effect. In fact, the tumor concentration of free SN-38 at 24 hours after administration of NK012 reached 90.4 ng/g and high concentrations were maintained up to 168 hours (53.1 ng/g for 48 hours, 42.6 ng/g for 72 hours, and 35.8 ng/g for 168 hours). This range of concentrations can exert sufficient antitumor activity against tumor cells. On the other hand, the concentration of CPT-11 was only 4.5 ng/g at 24 hours. These results indicate that the enhancement of tumor distribution closely contributes to the potent antitumor activity of NK012 *in vivo*.

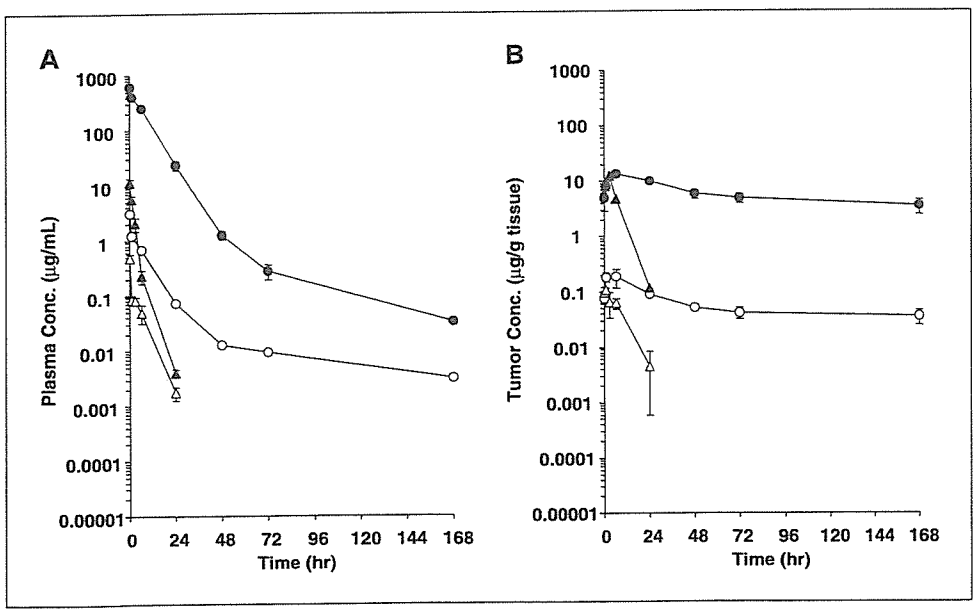

Figure 3. Plasma and tumor concentrations of respective analytes after an i.v. administration of CPT-11 (66.7 mg/kg) or NK012 (30 mg/kg) to HT-29-bearing nude mice. *A*, plasma. *B*, tumor. ●, polymer-bound SN-38; ○, free SN-38 (polymer-unbound SN-38); △, SN-38 converted from CPT-11; ▲, CPT-11.

Table 2. Pharmacokinetic variables of analytes in plasma and tumor after an i.v. administration of NK012 or CPT-11 to nude mice bearing human colon cancer HT-29 cells (NK012, 30 mg/kg; CPT-11, 66.7 mg/kg)

	Test article		C_{max} (μg/mL)	T_{max} (h)	$T_{1/2z}$ (h)	AUC_{last} (μg h/mL)	AUC_{inf} (μg h/mL)	CL_{tot} (mL/h/kg)	V_{ss} (mL/kg)	MRT_{last} (h)	$MRT_{inf.}$ (h)
Plasma	NK012	P-b SN-38*	—†	—	31.4	5,000	5,010	5.99	40.4	6.68	6.74
		P-u SN-38‡	3.10	0.0833	61.7	15.5	15.8	—	—	10.8	15.3
	CPT-11	CPT-11	—	—	3.08	22.1	22.2	3,010	5,420	1.78	1.80
		SN-38	0.488	0.0833	3.76	1.10	1.11	—	—	3.82	4.04
Tumor	NK012	P-b SN-38	13.8	6	—	1,010	—	—	—	62.8	—
		P-u SN-38	0.188	6	—	10.2	—	—	—	58.1	—
	CPT-11	CPT-11	12.6	3	3.36	99.7	100	—	—	4.41	4.55
		SN-38	0.108	1	4.75	1.07	1.10	—	—	5.20	5.92

NOTE: Three female nude mice were used for the analysis of biodistribution of SN-38 and CPT-11 in plasma and tissues. Data were expressed as means.
*Polymer-bound SN-38; SN-38 remaining bound to PEG-PGlu.
†Not determined.
‡Polymer-unbound SN-38; free SN-38 from PEG-PGlu.

Several preclinical studies on cytotoxic agent–incorporating polymeric micelles show their advantage as anticancer agents *in vivo* as compared with drugs of small molecular size (19, 22, 23). Because the advantage of passive targeting has been explained by the enhanced permeability and retention theory, it is essential to elucidate the correlation between the effectiveness of micellar drugs and tumor hypervascularity and hyperpermeability. We hypothesized that a polymeric micelle–based drug carrier could increase its accumulation in the tumor site and could thus enhance the therapeutic efficacy in tumors with high vascularity. To ascertain the hypothesis, we used SBC-3/VEGF. We adopted a bulky tumor model for our *in vivo* experiment to clarify the difference in activity against SBC-3/Neo and SBC-3/VEGF tumors. Histologic examination of SBC-3/VEGF showed hypervascularity and prominent leakage of erythrocytes. On the other hand, SBC-3/Neo showed hypovascularity. Our *in vivo* experiment showed that NK012 obviously enhanced its antitumor activity in SBC-3/VEGF-inplanted mice and eradicated bulky masses. It was thought that the sensitivity of cells to NK012 might not change *in vivo* because the *in vitro* sensitivity of NK012 was almost equivalent between SBC-3/Neo and SBC-3/VEGF cells. When we compared the distribution of NK012 (free SN-38) in the tumor sites, significantly enhanced accumulation was observed in the SBC-3/VEGF tumors. This strongly suggested that the drug distribution throughout the tumor site was enhanced by the hypervascularity and hyperpermeability induced by VEGF, and, subsequently, higher antitumor activity was achieved. High vascular density and enhanced vascular permeability might also be favorable for drug delivery of low molecular weight drugs. However, the SN-38 concentration was not significantly high in SBC-3/VEGF tumors after the administration of CPT-11, and tumors exhibited rapid regrowth after the treatment. We assume that such conventional low molecular size anticancer agents almost disappear from the bloodstream without being subjected to the enhanced permeability and retention effect before they can reach the target organs (solid tumor). The fact of correlation between the blood vessel density in

Table 3. Tumor-to-plasma concentration ratio (Kp) of analytes after an i.v. administration of NK012 (30 mg/kg) to nude mice bearing human colon cancer HT-29 cells

Test article	Analyte		Time after administration (h)						
			0.0833	1	6	24	48	72	168
NK012	P-b SN-38*	Plasma (μg/mL)	612	410	254	23.3	1.25	0.278	0.0333
		Tumor (μg/g)	4.99	8.00	13.8	9.95	5.90	5.03	3.58
		Kp† (mL/g)	0.00815	0.0195	0.0543	0.427	4.72	18.1	108
	P-u SN-38‡	Plasma (μg/mL)	3.10	1.24	0.673	0.0717	0.0127	0.00925	0.00325
		Tumor (μg/g)	0.0763	0.187	0.188	0.0904	0.0531	0.0426	0.0358
		Kp (mL/g)	0.0246	0.151	0.279	1.26	4.18	4.61	11.0

NOTE: Data were expressed as means of three mice.
*Polymer-bound SN-38; SN-38 remaining bound to PEG-PGlu.
†Kp values were calculated on the mean concentrations of three mice.
‡Polymer-unbound SN-38; free SN-38 from PEG-PGlu.

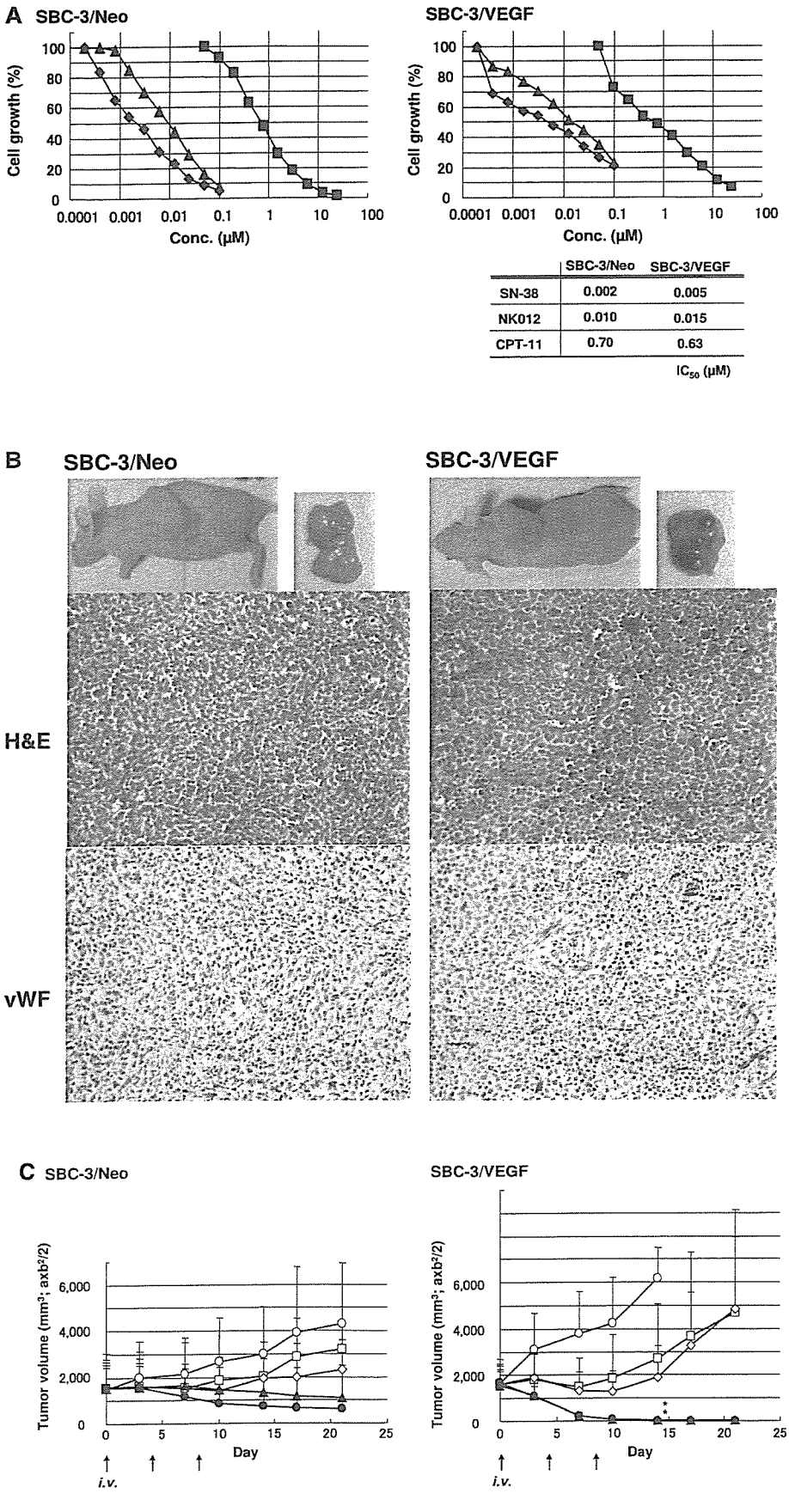

Figure 4. Growth inhibitory effect of NK012, SN-38, and CPT-11 on SBC-3/Neo and SBC-3/VEGF cells. *A*, in *in vitro* experiment, the cells were exposed to the indicated concentrations of each drug for 72 hours. The growth inhibition curves and IC_{50} values for NK012 (▲), SN-38 (◆), and CPT-11 (■) are shown. *B*, representative photographs of massive tumors developed from SBC-3/Neo and SBC-3/VEGF at the time just before treatment initiation. Histologic (H&E, ×20) and immunohistochemical (von Willebrand factor, ×20) examinations for each tumor are shown. *C*, i.v. administration of NK012 or CPT-11 was started when the mean tumor volumes of groups reached a massive size of 1,500 mm^3. The mice were divided into test groups (○, control; □, CPT-11 15 mg/kg/d; ◇, CPT-11 30 mg/kg/d; ▲, NK012 10 mg/kg/d; ●, NK012 20 mg/kg/d). NK012 or CPT-11 was administered i.v. on days 0, 4, and 8. Each group consisted of four mice. *, $P < 0.05$.

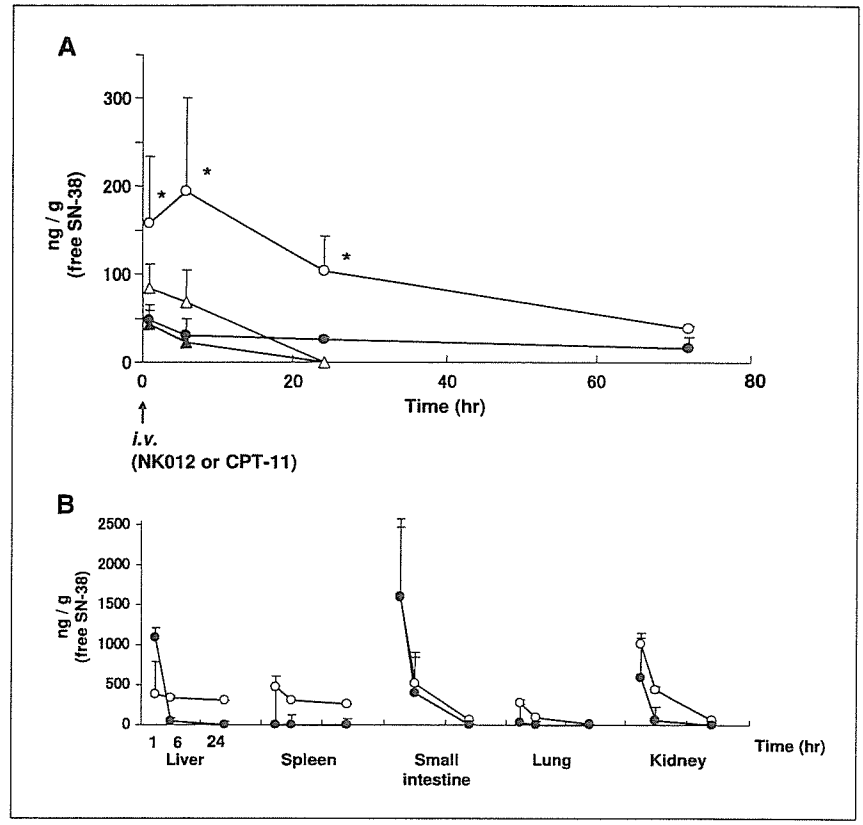

Figure 5. Tissue and tumor distribution of free SN-38 after administration of NK012 and CPT-11. *A*, time profile of free SN-38 concentration in SBC-3/Neo (●, NK012 20 mg/kg/d; ▲, CPT-11 30 mg/kg/d) and SBC-3/VEGF (○,NK012 20 mg/kg/d; △, CPT-11 30 mg/kg/d). NK012 on days 0 and 4 (96 hours) or CPT-11 on day 0 was administered. *, $P < 0.05$. *B*, tissue distribution of free SN-38 after single injection of NK012 at 30 mg/kg (○) and CPT-11 at 40 mg/kg (●).

the tumor mass and poor prognosis for survival in people with various types of cancers (25–28) supports the idea that low molecular weight drugs are not so effective in the treatment of solid tumors, which are rich in blood vessels.

Jain (35) reported that the convective passage of large drug molecules into the core of solid tumors could be impeded by abnormally high interstitial pressures in solid tumors. However, he also considered that low molecular weight anticancer agents might be harmful to normal organs because they can leak out of normal blood vessels freely; he finally concluded that one useful strategy for evading the barriers to drug dispersion would be to inject patients with drug carriers, such as liposome, filled with low molecular weight drugs. NK012 has the potential to allow the effective sustained release of SN-38 inside a tumor following the accumulation of NK012 into tumor tissue. As a matter of fact, substantial amount of SN-38 is expected to be released from the polymeric micelle. Consequently, released SN-38 becomes distributed throughout the tumor tissue and internalizes into cancer cells to kill them.

In recent years, the novel liposome-based formulation of SN-38 (LE-SN38) has been developed (36). LE-SN38 shows promising antitumor activity against various cancer cell lines (37, 38) and a clinical trial to assess its efficacy is now under way (39). The release of SN-38 from LE-SN38 is very slow as compared with NK012, ~1.9% of the drug being released from LE-SN38 in PBS buffer over 120 hours (36). The size of LE-N38 ranges from 150 to 200 nm. On the other hand, the particle size of NK012 is ~20 nm. Interestingly, Unezaki et al. (40) reported that fluorescence-labeled PEG liposomes were densely located outside the tumor vessels and stayed around the vessel walls for 2 days after i.v. injection. These data suggest that the PEG liposome is too large to move freely in the tumor interstitium and too stable to be released easily. The difference in size distribution and the character of the drug release between NK012 and LE-SN38 might influence their clinical effectiveness in the treatment of solid tumors.

One of the major toxicities associated with CPT-11 administration is severe diarrhea. Although the mechanism of the diarrhea has not yet been elucidated, one possible explanation is structural and functional injuries to the gastrointestinal tract owing to the mitotic inhibitory activity of SN-38 and CPT-11. It was reported that the number of episodes of diarrhea had a better correlation with the plasma AUC of SN-38 than with CPT-11 (41). In the present study, no difference in SN-38 accumulations in the small intestine was seen when equimolar NK012 (20 mg/kg) and CPT-11 (30 mg/kg) were administered. We also reported, using a rat mammary tumor model, that NK012 showed significant antitumor effect with diminishing incidence of diarrhea as compared with CPT-11 (42). These results suggest that diarrhea, one of the dose-limiting toxicities of CPT-11, is not augmented by the administration of NK012.

In conclusion, the present data suggest that NK012 possesses a treatment advantage over CPT-11, especially in hypervascular tumors such as renal cell carcinomas, medulloblastomas, and hepatocellular carcinomas. We have now started a phase I clinical trial for NK012 in patients with advanced solid tumors.

Acknowledgments

Received 5/3/2006; revised 7/20/2006; accepted 8/21/2006.

The costs of publication of this article were defrayed in part by the payment of page charges. This article must therefore be hereby marked *advertisement* in accordance with 18 U.S.C. Section 1734 solely to indicate this fact.

References

1. Li LH, Fraser TJ, Olin EJ, Bhuyan BK. Action of camptothecin on mammalian cells in culture. Cancer Res 1972;32:2643–50.
2. Gallo RC, Whang-Peng J, Adamson RH. Studies on the antitumor activity, mechanism of action, and cell cycle effects of camptothecin. Natl Cancer Inst 1971; 46:789–95.
3. Gottlieb JA, Guarino AM, Call JB, Oliverio VT, Block JB. Preliminary pharmacologic and clinical evaluation of camptothecin sodium (NSC-100880). Cancer Chemother Rep 1970;54:461–70.
4. Muggia FM, Creaven PJ, Hansen HH, Cohen MH, Selawry OS. Phase I clinical trial of weekly and daily treatment with camptothecin (NSC-100880): correlation with preclinical studies. Cancer Chemother Rep 1972;56: 515–21.
5. Cunningham D, Pyrhonen S, James RD, et al. Randomised trial of irinotecan plus supportive care versus supportive care alone after fluorouracil failure for patients with metastatic colorectal cancer. Lancet 1998; 352:1413–8.
6. Saltz LB, Cox JV, Blanke C, et al. Irinotecan plus fluorouracil and leucovorin for metastatic colorectal cancer. Irinotecan Study Group. N Engl J Med 2000;343: 905–14.
7. Noda K, Nishiwaki Y, Kawahara M, et al. Irinotecan plus cisplatin compared with etoposide plus cisplatin for extensive small-cell lung cancer. N Engl J Med 2002; 346:85–91.
8. Negoro S, Masuda N, Takada Y, et al. CPT-11 Lung Cancer Study Group West. Randomised phase III trial of irinotecan combined with cisplatin for advanced non-small-cell lung cancer. Br J Cancer 2003; 88:335–41.
9. Bodurka DC, Levenback C, Wolf JK, et al. Phase II trial of irinotecan in patients with metastatic epithelial ovarian cancer or peritoneal cancer. J Clin Oncol 2003; 21:291–7.
10. Takimoto CH, Arbuck SG. Topoisomerase I targeting agents: the camptothecins. In: Chabner BA, Lango DL, editors. Cancer chemotherapy and biotherapy: principal and practice. 3rd ed. Philadelphia (PA): Lippincott Williams & Wilkins; 2001. p. 579–646.
11. Slatter JG, Schaaf LJ, Sams JP, et al. Pharmacokinetics, metabolism, and excretion of irinotecan (CPT-11) following I.V. infusion of [(14)C]CPT-11 in cancer patients. Drug Metab Dispos 2000;28:423–33.
12. Rothenberg ML, Kuhn JG, Burris HA III, et al. Phase I and pharmacokinetic trial of weekly CPT-11. J Clin Oncol 1993;11:2194–204.
13. Guichard S, Terret C, Hennebelle I, et al. CPT-11 converting carboxylesterase and topoisomerase activities in tumour and normal colon and liver tissues. Br J Cancer 1999;80:364–70.
14. Matsumura Y, Maeda H. A new concept for macromolecular therapeutics in cancer chemotherapy: mechanism of tumoritropic accumulation of proteins and the antitumor agent smancs. Cancer Res 1986;46: 6387–92.
15. Dvorak HF, Nagy JA, Dvorak JT, Dvorak AM. Identification and characterization of the blood vessels of solid tumors that are leaky to circulating macromolecules. Am J Pathol 1988;133:95–109.
16. Maeda H, Matsumura Y. Tumoritropic and lymphotropic principles of macromolecular drugs. Crit Rev Ther Drug Carrier Syst 1989;6:193–210.
17. Matsumura Y, Maruo K, Kimura M, Yamamoto T, Konno T, Maeda H. Kinin-generating cascade in advanced cancer patients and *in vitro* study. Jpn J Cancer Res 1991;82:732–41.
18. Yokoyama M, Miyauchi M, Yamada N, et al. Characterization and anticancer activity of the micelle-forming polymeric anticancer drug Adriamycin-conjugated poly(ethylene glycol)-poly(aspartic acid) block copolymer. Cancer Res 1990;50:1693–700.
19. Yokoyama M, Okano T, Sakurai Y, Ekimoto H, Shibazaki C, Kataoka K. Toxicity and antitumor activity against solid tumors of micelle-forming polymeric anticancer drug and its extremely long circulation in blood. Cancer Res 1991;51:3229–36.
20. Kataoka K, Harada A, Nagasaki Y. Block copolymer micelles for drug delivery: design, characterization and biological significance. Adv Drug Deliv Rev 2001;47: 113–31.
21. Matsumura Y, Hamaguchi T, Ura T, et al. Phase I clinical trial and pharmacokinetic evaluation of NK911, a micelle-encapsulated doxorubicin. Br J Cancer 2004;91: 1775–81.
22. Hamaguchi T, Matsumura Y, Suzuki M, et al. NK105, a paclitaxel-incorporating micellar nanoparticle formulation, can extend *in vivo* antitumour activity and reduce the neurotoxicity of paclitaxel. Br J Cancer 2005; 92:1240–6.
23. Uchino H, Matsumura Y, Negishi T, et al. Cisplatin-incorporating polymeric micelles (NC-6004) can reduce nephrotoxicity and neurotoxicity of cisplatin in rats. Br J Cancer 2005;93:678–87.
24. Folkman J. Anti-angiogenesis: new concept for therapy of solid tumors. Ann Surg 1972;175:409–16.
25. Gasparini G, Harris AL. Clinical importance of the determination of tumor angiogenesis in breast carcinoma: much more than a new prognostic tool. J Clin Oncol 1995;13:765–82.
26. Dickinson AJ, Fox SB, Persad RA, Hollyer J, Sibley GN, Harris AL. Quantification of angiogenesis as an independent predictor of prognosis in invasive bladder carcinomas. Br J Urol 1994;74:762–6.
27. Takahashi Y, Kitadai Y, Bucana CD, Cleary KR, Ellis LM. Expression of vascular endothelial growth factor and its receptor, KDR, correlates with vascularity, metastasis, and proliferation of human colon cancer. Cancer Res 1995;55:3964–8.
28. Williams JK, Carlson GW, Cohen C, Derose PB, Hunter S, Jurkiewicz MJ. Tumor angiogenesis as a prognostic factor in oral cavity tumors. Am J Surg 1994; 168:373–80.
29. Natsume T, Watanabe J, Koh Y, et al. Antitumor activity of TZT-1027 (Soblidotin) against vascular endothelial growth factor-secreting human lung cancer *in vivo*. Cancer Sci 2003;94:826–33.
30. Stacker SA, Caesar C, Baldwin ME, et al. VEGF-D promotes the metastatic spread of tumor cells via the lymphatics. Nat Med 2001;7:186–91.
31. Amoroso A, Del Porto F, Di Monaco C, Manfredini P, Afeltra A. Vascular endothelial growth factor: a key mediator of neoangiogenesis. A review. Eur Rev Med Pharmacol Sci 1997;1:17–25.
32. Cabral H, Nishiyama N, Okazaki S, Koyama H, Kataoka K. Preparation and biological properties of dichloro(1,2-diaminocyclohexane)platinum(II) (DACHPt)-loaded polymeric micelles. J Controlled Res 2005;101: 223–32.
33. Nishiyama N, Yokoyama M, Aoyagi T, Okano T, Sakurai Y, Kataoka K. Preparation and characterization of self-assembled polymer-metal complex micelle from *cis*-dichlorodiammineplatinum(II) and poly(ethylene glycol)-poly(α,β-aspartic acid) block copolymer in an aqueous medium. Langmuir 1999;15:377–83.
34. Kawato Y, Furuta T, Aonuma M, Yasuoka M, Yokokura T, Matsumoto K. Antitumor activity of a camptothecin derivative, CPT-11, against human tumor xenografts in nude mice. Cancer Chemother Pharmacol 1991;28:192–8.
35. Jain RK. Barriers to drug delivery in solid tumors. Sci Am 1994;271:58–65.
36. Zhang JA, Xuan T, Parmar M, et al. Development and characterization of a novel liposome-based formulation of SN-38. Int J Pharm 2004;270:93–107.
37. Lei S, Chien PY, Sheikh S, Zhang A, Ali S, Ahmad I. Enhanced therapeutic efficacy of a novel liposome-based formulation of SN-38 against human tumor models in SCID mice. Anticancer Drugs 2004;15:773–8.
38. Pal A, Khan S, Wang YF, et al. Preclinical safety, pharmacokinetics and antitumor efficacy profile of liposome-entrapped SN-38 formulation. Anticancer Res 2005;25:331–41.
39. Kraut EH, Fishman MN, LoRusso PM, et al. Final result of a phase I study of liposome encapsulated SN-38 (LE-SN38): safety, pharmacogenomics, pharmacokinetics, and tumor response [abstract 2017]. Proc Am Soc Clin Oncol 2005;23:139s.
40. Unezaki S, Maruyama K, Hosoda JI, et al. Direct measurement of the extravasation of polyethyleneglycol-coated liposomes into solid tumor tissue by *in vivo* fluorescence microscopy. Int J Pharmaceut 1996;144: 11–7.
41. Sasaki Y, Yoshida Y, Sudoh K, et al. Pharmacological correlation between total drug concentration and lactones of CPT-11 and SN-38 in patients treated with CPT-11. Jpn J Cancer Res 1995;86:111–6.
42. Onda T, Nakamura I, Seno C, et al. Superior antitumor activity of NK012, 7-ethyl-10-hydroxycamptothecin-incorporating micellar nanoparticle, to irrinotecan [abstract 3062]. Proc Am Assoc Cancer Res 2006;47: 720s.